Journal of Iberian Geology
https://doi.org/10.1007/s41513-023-00207-9

RESEARCH PAPER

Quaternary fluvial carbonate deposits of the Almonda River Valley, Central Portugal

João Paulo Fernandes[1] · Concha Arenas[2] · José Eugenio Ortiz[3]

Received: 30 December 2022 / Accepted: 10 February 2023

Abstract

This paper discusses the formation and preservation of a fluvial tufa system influenced by Atlantic climate based on stratigraphical, chronological (amino-acid racemization, AAR), sedimentological and stable-isotope analyses. On the southwestern Iberian Peninsula, the tufas and associated deposits of the Almonda River valley occur as isolated terraced bodies and reach 25 m thick. AAR dated most deposits to within the warm Marine Isotope Stage 5 (MIS-5). Two Holocene ages were reset within MIS-5 based on diverse criteria. Widely varied carbonate and minor allochthonous coarse detrital facies occur arranged in four simple vertical associations. The deposit geometry and facies association distribution correspond to a low- to moderate-sloped fluvial valley consisting of several short knickpoints and extensive flat areas between them. The latter are occupied by slow-flowing water facies (carbonate sand, lime mud, phytoclast and oncoid rudstones, and up-growing stem boundstones). Facies that formed in moderate- to high-slope substrates were stromatolite, moss and down-growing stem boundstones. The homogeneous Miocene bedrock lithology and gentle structural deformation propitiated this depositional architecture. Calcite $\delta^{13}C$ and $\delta^{18}O$ values suggest that the aquifer water provided the outflowing Almonda water with (1) ^{18}O-enriched water, compared with present precipitation and groundwater $\delta^{18}O$ values, and (2) ^{13}C-depleted CO_2 from bituminous rocks and vegetation cover in the catchment. The proximity to the Atlantic coast favoured the Mesozoic-rock aquifer recharge with ^{18}O-enriched water precipitation, assuring water availability during the formation of the studied tufas. No evidence of frequent intense erosion phases might indicate stable precipitation regimes, which would have allowed the preservation of loose fine-grained and palustrine deposits.

Keywords Fluvial tufas · Sedimentary facies model · Atlantic climate · Pleistocene · Iberia

Depósitos fluviales carbonatados cuaternarios del valle del río Almonda, centro de Portugal

Resumen

En este trabajo se discuten los factores de formación y conservación de un sistema fluvial tobáceo influenciado por clima atlántico, basado en análisis estratigráficos, cronológicos (Racemización de Amino Ácidos, RAA) y sedimentológicos,

✉ Concha Arenas
carenas@unizar.es

[1] Department of Education, Culture and Sport, Torres Novas Municipality1 Largo das Forças Armadas St, 2350-754 Torres Novas, Portugal

[2] Department of Earth Sciences, Institute for Research on Environmental Sciences of Aragón (IUCA) and GeoTransfer Group, University of Zaragoza, 12 Pedro Cerbuna St, 50009 Zaragoza, Spain

[3] Laboratory of Biomolecular Stratigraphy. Higher Technical School of Mining Engineers, Polytechnic University of Madrid, 21 Ríos Rosas St, 28003 Madrid, Spain

Published online: 18 March 2023

complementados con análisis de isótopos estables. En el suroeste de la Península Ibérica, las tobas y depósitos asociados del valle del río Almonda forman cuerpos aterrazados aislados, de hasta 25 m de potencia. La RAA dató la mayoría de los depósitos dentro del estadio isotópico cálido 5 (MIS-5). Dos datos holocenos se reinterpretaron dentro del MIS-5 según diversos criterios. Las facies carbonatadas son variadas y junto con los escasos detríticos groseros alóctonos se organizan en cuatro asociaciones verticales simples. La geometría de los depósitos y la distribución de esas asociaciones de facies corresponde a un valle fluvial de moderada a baja pendiente, formado por pequeños saltos y extensas áreas planas entre ellos. Estas últimas, ocupadas por facies de flujo de agua lento (arena carbonatada, barro carbonado, rudstones de fitoclastos y oncoides, y boundstones de tallos creciendo hacia arriba). En los sustratos de pendiente moderada a alta se formaron estromatolitos y boundstones de musgos y de tallos colgantes. La homogeneidad litológica y estructural del sustrato mioceno habría propiciado esa arquitectura de depósito. Los valores de $\delta^{13}C$ y $\delta^{18}O$ sugieren que el acuífero proporcionó al agua del río Almonda: (1) CO_2 pobre en ^{16}O, comparando con el $\delta^{18}O$ de la precipitación y agua subterranean actual, y (2) CO_2 rico en ^{12}C, derivado de rocas bituminosas y la vegetación de la cuenca de recepción. La proximidad a la costa atlántica favoreció la recarga del acuífero de rocas mesozoicas con precipitación de agua rica en ^{18}O, además de asegurar la disponibilidad de agua durante la formación de las tobas estudiadas. La falta de evidencias de frecuentes fases de erosion intensa podría indicar regímenes de precipitación estables, que habrían favorecido la conservación de los depósitos de grano fino y palustres.

Palabras clave Tobas fluviales · Modelo de facies sedimentarias · Clima atlántico · Pleistoceno · Iberia

1 Introduction

Tufas are calcium carbonate rocks, mainly calcite, that form in terrestrial environments, such as streams, lakes and springs (Capezzuoli et al., 2014; Pedley, 1990). Freshwater carbonate-depositing rivers and lakes are the most common contexts for tufa formation, but saline and alkaline lakes may also be loci for tufa formation (Della Porta, 2015; Pentecost, 2005; Renaut et al., 2013). These limestones result from calcite precipitation on diverse biotic substrates, primarily through CO_2 loss from water caused by changes in temperature, biological processes and/or mechanical agitation (Pentecost, 2005). Tufa-associated carbonate sediments are commonly included within the term "tufa", as is the case for oncolites and stromatolites.

In mid-latitude regions, tufas developed extensively through the interglacial Quaternary periods (i.e., time periods correlative to odd marine isotope stages, MISs; e.g., Gibbard et al., 2005), which were characterized by warm conditions, with prominent deposits at approximately 100 ka (corresponding to MIS 5), as shown by the works of Martín Algarra et al. (2003), Torres et al. (2005), Ortiz et al. (2009) and Sancho et al. (2015). However, tufa formation has been found to occur in more varied climate conditions, ranging from temperate–wet to semiarid and arid (Cremaschi et al., 2010; Kele et al., 2021; Moeyersons et al., 2006; Stone et al., 2022; Viles et al., 2007). In fact, some tufa deposits in the Iberian Range formed during MISs 8 and 6 (Torres et al., 2005; Valero-Garcés et al., 2008; Sancho et al., 2015)—two "glacial" periods—. Together, these facts suggest that factors other than climate can also influence tufa formation (Viles & Pentecost, 2007), such as the bedrock lithology, the characteristics of the related aquifer, and basin slope variations along water flow directions (Arenas-Abad et al., 2010). Moreover, intrinsic factors, such as flora development and physical and chemical characteristics of water, may play a crucial role in some characteristics of tufa deposits, such as the type of facies and the geometry and thickness of the deposits (Arenas et al., 2014a, 2014b; Arenas-Abad et al., 2010; Violante et al., 1994).

Some studies have focused on the palaeoclimatic significance of tufas because their formation appears to be favoured in warm (Durán, 1989; Henning et al., 1983; Martín Algarra et al., 2003; Ortiz et al., 2009) and/or humid conditions (Capezzuoli et al., 2010). However, it is important to note that most of the abovementioned climate-related contributions are based on knowledge of the age of the deposits, but for the most part, the tufa attributes per se do not allow us to decipher the precise climate conditions during their formation. However, in a few cases, climate conditions have been described based on particular features of flora and/or fauna in tufas (Martínez-Tudela et al., 1986; Ricci et al., 2015; Roiron, 1997; Rubio-Millán, 2002; Bertini et al., 2014; Aranbarri et al., 2021).

There are few known examples of the influence of climate on tufa formation during Quaternary interglacials in the European region influenced by Atlantic climate. Except for a few notes describing tufas in Portugal (e.g., Choffat, 1895; Flyche, 1907; Mendes, 1974; Soares et al., 1997) or as part of other geomorphological studies (e.g., Santos, 1996), the first works considering sedimentary, geochemical and/or paleontological aspects with hydrological and climatic implications in central Portugal are by Queiroz and Mateus (2011) and Ribeiro et al., (2013, 2014). To the south of the study area, Guerreiro (2013, 2015) and Guerreiro et al. (2010) described different tufa facies in Quaternary deposits in the central Algarve. Facies associations were interpreted in relation to geomorphological

features and water flow conditions, fitting the stepped fluvial models of Arenas-Abad et al. (2010). Pedley et al. (1996) compared Holocene barrages from Spain and Britain and suggested that the "different characteristics of their preserved fabrics should allow recognition of two contrasting *climatic* models for fluvial barrage tufas in ancient deposits". Azennoud et al. (2021) demonstrated the response of tufas to climate on the multi-centennial time-scale over the last 5000 years in northwestern Africa.

This work presents the results of a study of Quaternary tufas and tufa-associated deposits in the Almonda River valley (central part of Portugal; Fig. 1A, B) based on stratigraphic, chronological and sedimentological analyses, along with stable isotope analysis of the carbonate facies. The main objectives were (1) to interpret the depositional stages based on stratigraphic and numerical dating criteria, (2) to characterize the depositional system through facies analysis and provide a sedimentary facies model, and (3) to discuss the factors that influenced the formation of the carbonate and associated deposits in that region. This is the first study that assesses the depositional, hydrological and climatic significance of fluvial tufas in this region, providing new information that can help sedimentological and climatic interpretations elsewhere. Moreover, this study is intended to highlight the potential of tufa as an educational and touristic resource in the Iberian Peninsula.

2 Geographical and geological location

The study area is located in the central part of Portugal, 95 km to the northeast of Lisbon, in an area known as *Médio Tejo or Ribatejo* (Fig. 1A). The studied Quaternary tufas and associated deposits crop out along the WNW–ESE-oriented stretch of the Almonda River valley (Fig. 2). The Almonda River is a direct tributary of the Tagus River. It flows from west to east for 13.8 km and then turns and flows north to south for 20.4 km. The altitude range from 75 m above sea

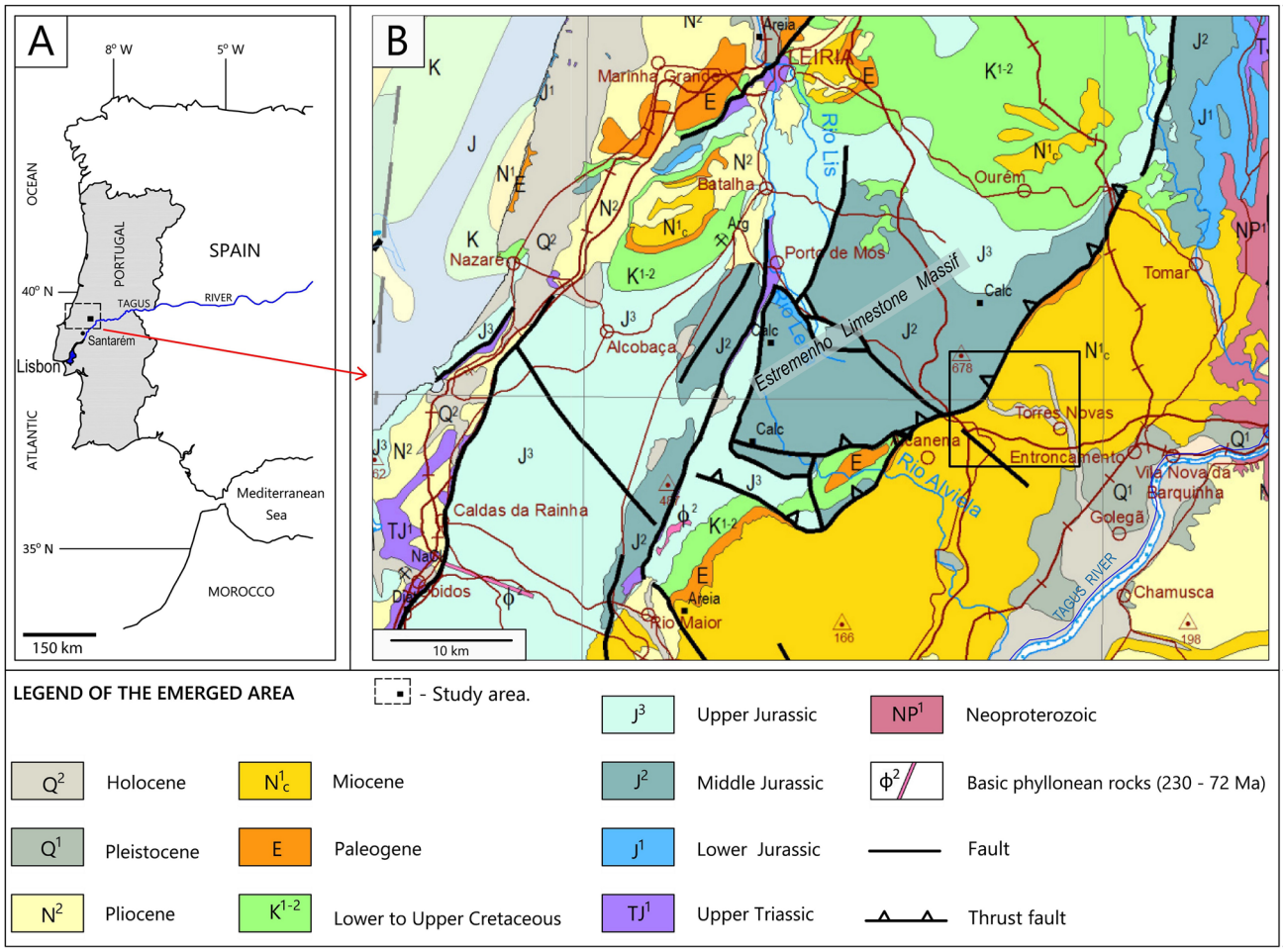

Fig. 1 Geographical and geological location. **A** Location of the study area in the Iberian Peninsula, central part of Portugal. **B** General geology of the study area. Adapted from the Geological Map of Portugal, scale 1:1,000,000 (Duarte & Bento dos Santos, 2010)

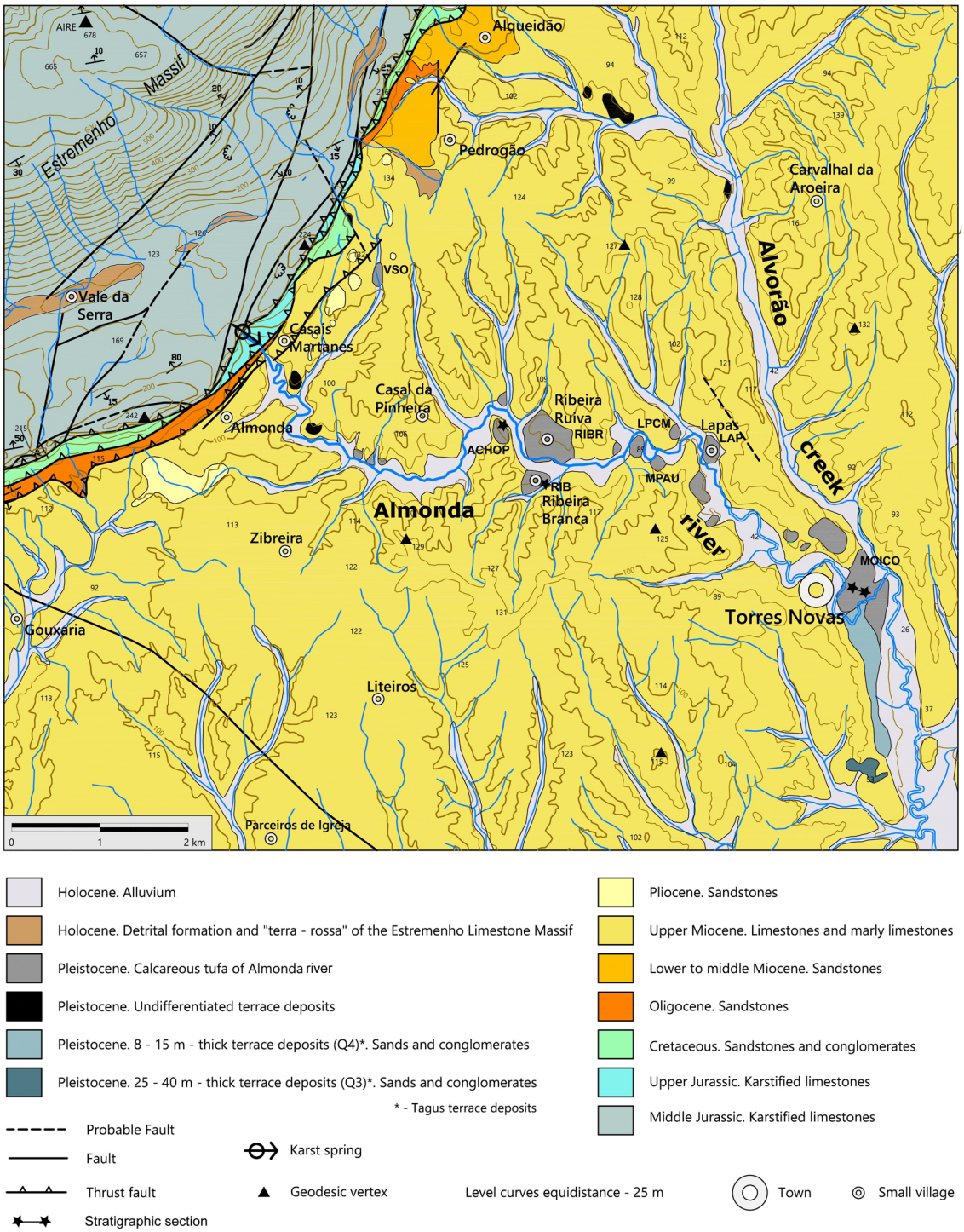

Fig. 2 Map of Quaternary tufas and related deposits in the WNW–ESE stretch of the Almonda River valley. Miocene strata are gently dipping southeastward and horizontal. Adapted from 1:50,000 geological sheets n. 27 – A (Vila Nova de Ourém; Manuppella et al., 2000) and n. 27 – C (Torres Novas; Manuppella et al., 2006), of the *Instituto Geológico e Mineiro* of Portugal

level (asl) at the uppermost spring to 28 m asl at its joining with a northflowing stream (Alvorão valley), close to the locality of Torres Novas. The Almonda River enters the Tagus River 20.4 km downstream of Torres Novas at 15 m asl (Fig. 1B).

The present climate of the region is temperate, with rainy winters and dry, mild summers upstream of the source of

the Almonda River (Estremenho Limestone Massif), and with rainy winters and dry, hot summers downstream of the Almonda source (https://www.ipma.pt/pt/educativa/tempo.clima/index.jsp?page=clima.pt.xml).

Data from Santarém (30 km south of Torres Novas in the Tagus Basin; Fig. 1A) provide the maximum average temperature of the hottest month of summer around 30 °C and the minimum average temperature of the coldest month of winter around 6 °C. It is normal to have maximum temperature peaks in the summer above 40 °C (Instituto Português do Mar e da Atmosfera, I. P., IPMA, I. P.; Fino, 2018).

The average precipitation in the region is higher in autumn and winter than in spring, with minima in summer. The average monthly data compiled from the Ribatejo region by Fino (2018) indicated that precipitation ranged between 295 mm (autumn), 220 mm (winter), 125 mm (spring) and 45 mm (summer) since 2006–2014.

Most of the river path is meandering (Manuppella et al., 2000) (Fig. 2). The alluvial plain can reach up to 300 m wide. In four sections of the river, the meanders tend to form abandoned stretches (oxbow lakes).

The mean river slope along the WNW–ESE stretch is approximately 0.34%, although it is highly variable along the valley. It increases significantly from kilometre 8 to the Torres Novas locality, reaching up to 5.5% between Lapas and Torres Novas. From Torres Novas, the river flows downhill with an average slope of 0.06%, as far as the Tagus River (Fig. 3). There are three knickpoints along the river: immediately after the source, between Lapas and Torres Novas and in Torres Novas. However, these points may have been changed by the recent construction of dams and weirs.

Jurassic limestone rocks crop out to the northwest in the Estremenho Limestone Massif (Figs. 1B, 2), a geomorphological unit with an extent of approximately 800 km^2, and this massif is high above the Cenozoic Tagus Basin. These rocks constitute an important and complex aquifer system with typical karst behaviour. The Miocene rocks of the Tagus Basin consist of limestones, marly limestones and marls, with sandstone and mudstone intercalations corresponding to lateral facies variations (Manuppella et al., 2000). These rocks are widely represented to the east and south of the Jurassic outcrop. The contact between these two geological units is a fault (Arrifes thrust), through which the two main perennial karst springs from the massif, namely, the outflows of the Alviela and Almonda Rivers, are located, with average values of water flow from the karst system of 120 hm^3/year and 80–100/hm^3/year, respectively (Almeida et al., 2000). The chemical composition of the river water is of the calcium bicarbonate type (Almeida et al., 2000; Manuppella et al., 2006).

The Quaternary tufa deposits that crop out along the WNW–ESE stretch of the Almonda River valley and some of its tributaries, from the upstream springs to the locality of Torres Novas, are studied in this paper. These deposits unconformably overlie the Miocene bedrock and appear incised by the present Almonda River (Figs. 2, 3). The contact between the Miocene bedrock and the tufa and associated carbonate and detrital deposits is not always observable. These tufa deposits crop out as terraced isolated build-ups along the present-day Almonda River valley and a few isolated deposits in one lateral tributary valley (Figs. 2, 3). Some close tufa outcrops correspond to

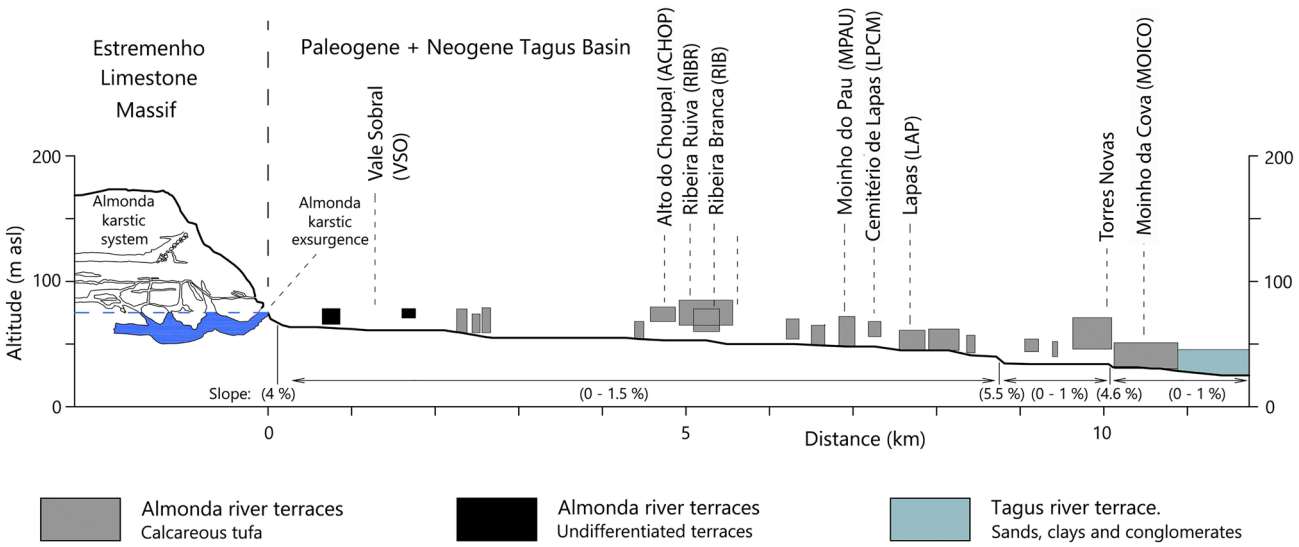

Fig. 3 Longitudinal profile of the Almonda River and tufa altitude across a WNW−ESE section (from the upstream spring to the south of Torres Novas town) adapted from Thomas (1985). The Vale Sobral tufa creek on the north bank (VSO) is also projected. The location is shown in Fig. 2

the same build-up that has been dissected by the present river (e.g., the Ribeira Ruiva and Ribeira Branca outcrops) (Fig. 2). Tufa deposits occur approximately 2.5 km from the main water source, which is located at the contact with the Jurassic rocks. The altitude of the base of the outcropping deposits ranges from 59 m (terrace close to Casal da Pinheira) to ca. 28 m (terrace of Moinho da Cova, in Torres Novas) (Fig. 2).

The Lapas locality is built on an extensive tufa build-up, whose interior observation is possible through a series of artificial tunnels excavated in the tufa in the past. The tunnels occur in the middle part of the Lapas build-up, with vertical conduits (chimneys) that reach the surface at an elevation of 60 m asl. The lowest tunnels were opened at an elevation of 50 m asl. The labyrinthic transect spans approximately 400 m long. These tunnels and other close tunnels in the area have been considered of public interest since 1943, and have formed part of the *Roteiro das Minas e Pontos de Interesse Mineiro e Geológico de Portugal* since 2019.

3 Materials and methods

Tufa and associated deposits in the study area were mapped on a 1:10,000 topographic basis by superposing information of the 1:50,000 geological sheets n. 27—A (Vila Nova de Ourém; Manuppella et al., 2000) and n. 27—C (Torres Novas; Manuppella et al., 2006) (Fig. 2). Three stratigraphic sections (ACHOP–Alto do Choupal–, MOICO–Moinho da Cova–, and RIB–Ribeira Branca–) were measured and located on a 1:10,000 topographic basis. Several other outcrops were also studied. Correlation between the several outcropping deposits was based on mapping, lateral continuity of outcrops and the ages provided by amino acid racemization (explanation given below). Sedimentological drawings of diverse outcrops were also made based on photographic mosaics.

From the measured sections and several other outcrops, 42 samples were selected based on their stratigraphic position and lithofacies types for diverse types of analyses, including their textural, mineralogical and stable isotope characteristics, and dating. Twenty-five thin sections were prepared for the textural characterization through petrographic microscope observations, and 8 samples (whose approximate dimensions are 5 × 5x3 mm) were prepared for scanning electron microscopy (SEM). The thin sections were made at the *Servicio General de Preparación de rocas y materiales duros, impresión y escaneado en 3D* of the *Servicio General de Apoyo a la Investigación* (SAI) of the University of Zaragoza (Spain). The SEM facility was a Carl Zeiss MERLIN™ FESEM; Zeiss AG, operating at 3 to 15 kV and 158 pA, which belonged to the *Servicio de Microscopía electrónica de materiales* of the SAI.

The classification codes of Miall (1978) have been used for the clastic facies (i.e., rocks formed of extraclasts), and the classification codes of Arenas-Abad et al. (2010) have been used for the carbonate facies.

3.1 Amino acid racemization (AAR)

A total of 9 samples from 9 beds corresponding to carbonate silts and sands located in six different tufa deposits (Fig. 4) were used for amino acid racemization (AAR) dating in the Biomolecular Stratigraphy Laboratory at the Polytechnic University of Madrid.

A total of 17 ostracod valves from 7 beds were analysed (Table 1). The valves were carefully sonicated and cleaned with water to remove sediment. They were then left for 3 h in hydrogen peroxide to eliminate organic matter. Only clean and translucent shells were selected from each sample. In addition, a small sample near the aperture of gastropod shells belonging to the *Theba* genus (Helicidae family) was recovered in 4 specimens from 2 samples (Table 2). In all cases, peripheral parts (approximately 20–30%) were removed after chemical etching with 2 N HCl. Afterwards, 10–20 mg of sample was selected for amino acid racemization analysis.

Amino acid concentrations were quantified using high-performance liquid chromatography following the sample preparation protocol described in Kaufman and Manley (1998) and Kaufman (2000). This procedure involves hydrolysis, which was performed under a N_2 atmosphere in HCl for 20 h at 100 °C. The hydrolysates were evaporated to dryness in vacuo and then rehydrated in 7 mL (ostracodes) or in 10 µL/mg (gastropods) of 0.01 M HCl with 1.5 mM sodium azide and 0.03 mM L-homo-arginine (internal standard).

Samples were injected into an Agilent HPLC-1100 liquid chromatograph equipped with a fluorescence detector. Excitation and emission wavelengths were programmed at 230 nm and 445 nm, respectively. A Hypersil BDS C18 reverse-phase column (5 µm; 250 × 4 mm i.d.) was used for the analysis.

The age of a single bed is the average of the numerical dates obtained for each amino acid D/L value measured in gastropods or ostracods from that level, and the age uncertainty is the standard deviation of the numerical ages calculated at each level. The D/L nomenclature refers to the position of the NH_2 group to the right (D isomer) or to the left (L isomer).

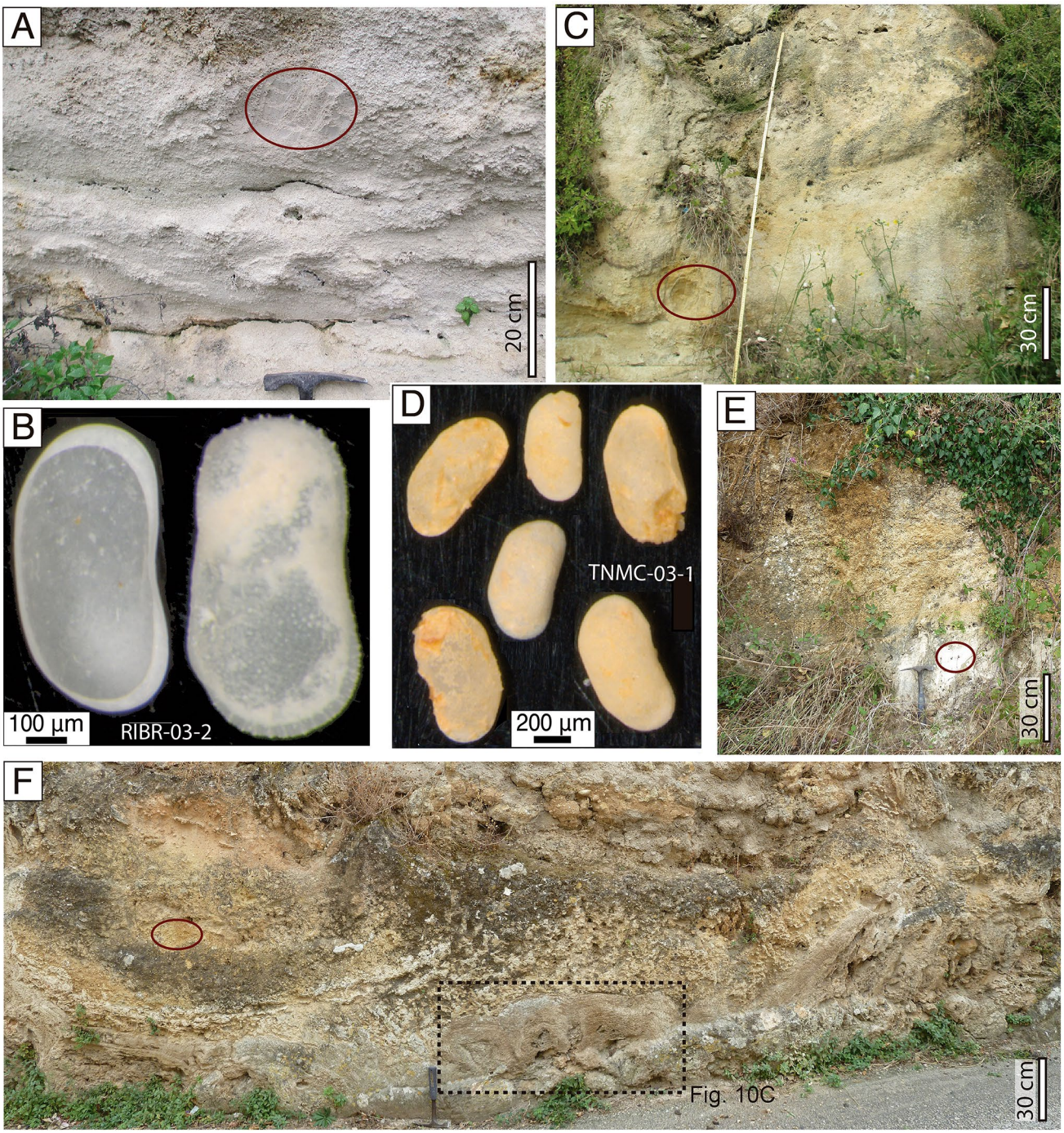

Fig. 4 Field images of sampled outcrops and ostracod specimens used for AAR. In all cases, sediment samples correspond to sand and silt carbonate sediment. **A** Ribeira Ruiva (sample RIBR-03). **B** Ostracods from sample taken in **A**. **C** Lapas (sample LAP-01). **D** Ostracods from sample taken in **F**. **E** Moinho do Pau (sample MPAU). **F** Moinho da Cova (sample TNMC 03). Red ovals mark the sampled areas. For samples, refer to Tables 1 and 2 and Fig. 2

3.2 Stable isotope analysis

A total of 14 samples representing diverse facies from two sections were obtained through a microdrill and a punch and then ground and sieved to 62 µm, for C and O stable isotope analyses. $\delta^{13}C$ and $\delta^{18}O$ were determined at the *Servicios Científico-Técnicos* (CCIT-UB Serveis) of the University of Barcelona (Spain). The isotopic ratios were measured in a mass spectrometer (MAT-252, Thermo Finnigan; Thermo Fisher Scientific, Waltham,

Table 1 Aspartic acid (Asp) and glutamic acid (Glu) D/L values in ostracod valves of carbonate samples (facies Sb) and corresponding ages

Sample	Ostracode	N	D/L Asp	D/L Glu	Age (yr)
MPAU	*Cypris*	2	0.111	0.026	1345
LAP 02	*Candona*	1	–	–	–
RIBR 01	*Candona*	2	–	–	–
RIBR 03	*Ilyocypris*	1	0.366	0.105	112,400 ± 12,100
TNMC 01	*Herpetocypris*	5	–	–	–
TNMC 03	*Candona*	2	0.293	0.059	8975
LPCM 01	*Herpetocypris*	4	0.348 ± 0.001	0.133 ± 0.019	121,100 ± 14,700

Table 2 Aspartic acid (Asp). glutamic acid (Glu), leucine (Leu) and isoleucine (Ile) D/L values in gastropod shells (Helicidae) of carbonate samples (facies Sb) and corresponding ages

Sample	Gastropod	N	D/L Asp	D/L Glu	D/L Leu	D/L Ile	Age (yr)
RIB-1	*Theba*	2	0.554 ± 0.046	0.366 ± 0.039	0.422 ± 0.010	0.339 ± 0.024	124,380 ± 20,480
RIB-2	*Theba*	2	0.540 ± 0.044	0.330 ± 0.050	0.522 ± 0.010	0.394 ± 0.010	116,200 ± 28,370

Table 3 Values of $\delta^{13}C$ versus $\delta^{18}O$ (‰ V-PDB) of calcite samples, indicating the corresponding sedimentary facies

Facies	Sample	$\delta^{13}C$(PDB) ‰ V-PDB	$\delta^{18}O$(PDB) ‰ V-PDB
Lph, Lst1	MOICOb-1	− 10.10	− 4.96
Lbr	MOICOb-6	− 10.41	− 4.62
Ls	MOICOb-8	− 10.55	− 5.27
Lph	MOICO-2	− 10.21	− 4.07
Lbr	MOICO-4	− 10.43	− 4.65
Lst2	MOICO-5	− 9.56	− 4.21
Ls/Lbr	MOICO-9	− 9.68	− 4.39
Ls	MOICO-20	− 10.33	− 4.61
Ls	MOICO-21	− 10.33	− 4.49
Lb (Ch)	ACHOP-2b	− 10.28	− 4.76
Lbr	ACHOP-3	− 9.10	− 4.58
Ls (Lsp)	ACHOP-4	− 7.97	− 4.26
Lphf	ACHOP-6	− 10.84	− 4.08
Lbr	ACHOP-7	− 10.56	− 4.25

See Fig. 14B for the legend of symbols

MA, USA) via CO_2 obtained in a Carbonate Kiel Device III (Thermo Finnigan) by the reaction of samples with 100% H_3PO_4 at 70 °C for 3 min (McCrea, 1950). The international standards NBS-19 was used ($\delta^{13}C = 1.95$‰; $\delta^{18}O = -2.20$‰ V-PDB). The overall reproducibility was better than 0.02‰ for $\delta^{13}C$ and 0.04‰ for $\delta^{18}O$. The results are reported in δ‰ notation relative to Vienna Pee Dee Belemnite (V-PDB) (Table 3).

4 Results

4.1 Amino acid racemization results

To establish the numerical ages of the ostracod samples used for AAR, aspartic acid (Asp) and glutamic acid (Glu) were selected because they account for a significant percentage (> 50%) of the amino acid content of most ostracod valves (Kaufman, 2000; Ortiz et al., 2013). Other amino acids were not considered due to their low racemization rates. The mean Asp and Glu D/L values in ostracod valves from the samples are shown in Table 1.

Of the ostracod samples, 8 results were excluded because the Asp and Glu D/L values were off of the covariance trend (cf. Kaufman, 2003, 2006) and/or because of abnormally high D/L values, characterized by Asp D/L and Glu D/L values plotting outside the 2σ range of the group (cf. Hearty et al., 2004; Kosnik & Kaufman, 2008). Specifically, we excluded 1 MPAU sample; 1 LAP 02 sample; 2 RIBR 01 samples; 1 TNMC 01 sample; 2 LPCM 01 samples, and 1 TNMC 03 sample.

For dating ostracod samples, we applied the age calculation algorithms described by Ortiz et al. (2004) for samples with Asp and Glu D/L values greater than 0.27 and 0.08, respectively. For the age calculation of ostracods of samples MPU and TNMC 03, we used the age calculation algorithm defined by Ortiz et al. (2015) for samples with Asp D/L values lower than 0.30 (Holocene samples): age (yr) = 17.74 D/L Asp – 0.90. In this latter case, we considered only Asx because it is the amino acid that racemises the fastest, and D/L Glu values are not able to discriminate Holocene ages (Ortiz et al., 2015).

To establish the amino chronology of the Helicidae shells from the carbonate deposits, we used the Asp, Glu, leucine (Leu), and isoleucine (Ile) contents, according to Goodfriend (1991). The analysis of more than one amino acid provides largely redundant information on the sample age. The mean Asp, Glu, Leu and Ile D/L values at each tufa level are shown in Table 2 together with their ages.

The numerical age of the *Theba* shells at each level was calculated by introducing the Asp, Glu, Leu and Ile D/L values into the age calculation algorithms established by Torres et al. (1997) for gastropods in the central and southern parts of the Iberian Peninsula.

The ages provided by AAR are shown in Tables 1 and 2. Most analysed samples are Middle-Late Pleistocene in age, between 124.38 ± 20.48 ka and 112.4 ± 12.1 ka, i.e., within MIS 5, and likely 5e. Two younger samples correspond to the Holocene, with two disparate ages: 1.35 ka (MPAU) and 8.97 ka (sample TNMC 03), within MIS 1 (Fig. 4).

4.2 Stratigraphy

The studied Quaternary record overlies Miocene rocks, although in some cases the base of the Quaternary deposits does not crop out. Figures 5, 6, 7, 8, 9 present three representative sections (Alto do Choupal, Ribeira Branca and Moinho da Cova, abbreviated as ACHOP, RIB and MOICO, respectively, Figs. 5, 6 and 9), along with field images of some conspicuous characters. The studied deposits are dominated by limestones and carbonate sands and silts, which, in some cases, are found to lie over less abundant clastic deposits formed of conglomerates and gravels (e.g., Alto do Choupal, ACHOP, Fig. 5A, F). The thicknesses of some build-ups and sections vary between a few metres (e.g., in the Vale Sobral, VSO section, and Ribeira Branca, RIB section, Figs. 2, 6, 8) and up to 23 m (e.g., in Moinho da Cova, MOICO section, Fig. 9A), although some build-ups can be thicker than the measured sections, e.g., at Ribeira Branca, up to 23 m thick (Fig. 3). All outcropping deposits are physically disconnected. Thus, the relative stratigraphic position of these deposits can be established only by combining geological mapping and absolute dating. The ages obtained through AAR in several silty and sandy carbonate deposits herein allow us to separate two chronological groups of deposits (Tables 1, 2):

1) Pleistocene deposits. Most tufa build-ups in the study area coincide with the time of MIS 5 (i.e., Middle-Late Pleistocene). Precise stratigraphic correlation between the several Pleistocene build-ups and between the measured sections has not been possible (Figs. 5, 6, 9), as the obtained AAR ages overlap.
2) Holocene deposits. These deposits include the uppermost part of the MOICO build-up over an erosional surface, with an age of 8.97 ka, and the MPAU build-up (sample taken close to the base of the section), with an age of 1.35 ka. However, the AAR ages of these two build-ups are not fully consistent with their geomorphological and topographical positions relative to the surrounding dated deposits.

Below is a summary of the main stratigraphic characteristics of the most representative build-ups, including chronological considerations of some of them. Individual facies description and facies labels in the following summary are found in Table 4.

4.2.1 Middle-Late Pleistocene deposits

These deposits crop out along the main valley and represent the majority of the Quaternary tufa record. Although not all deposits could be dated due to the lack of suitable samples or due to the above-described technical problems relative to the AAR method, their topographic and stratigraphic positions relative to other dated tufa build-ups and alluvial terraces allowed us to tentatively assign them an approximate age.

This is the case of the Alto do Choupal build-up (ACHOP), which is ca. 15 m thick, along the middle stretch of the Almonda valley. The proximity and position of this build-up relative to the dated Ribeira Branca (RIB) and Ribeira Ruiva (RIVR) build-ups (Fig. 2) allowed us to place it within MIS 5. Figure 5 shows a stratigraphic section and field images of the ACHOP outcrop. Polygenic conglomerates crop out at the base, on Miocene marls (Fig. 5A, F, G).

The Ribeira Branca and Ribeira Ruiva build-ups, which are set in front of each other and separated by the present river, are 23 and 22 m thick, respectively (Figs. 2 and 4). The former yielded two close ages, 116.2 ± 28.37 and 124.38 ± 20.4 ka, and the latter yielded 112.4 ± 12.1 ka (Tables 1 and 2). Figures 6 and 7 show a stratigraphic section and illustrate the outcrops. Both lie on Miocene beds: coarse carbonate sands containing dispersed millimetre- to centimetre-long clasts in the northern RIB outcrop (Fig. 7A, B) and conglomerates at the base of the RIBR build-up occur on Miocene nodulised marly-limestones (Fig. 7A, B, C).

The deposits over which the Lapas locality is located (Lapas terrace) are another example of Pleistocene tufas. This build-up is up to 16 m thick. It stands out because of the extensive and intricate development of elongate caves (i.e., tunnels) carved mostly in fine-grained carbonate-dominated deposits, i.e., composed of fine phytoclasts (Lphf), small oncoids and sands (Lo, Sb), and stem boundstones (Lst 1) (Fig. 7E, F) (Fernandes, 2018). The Lapas cemetery terrace,

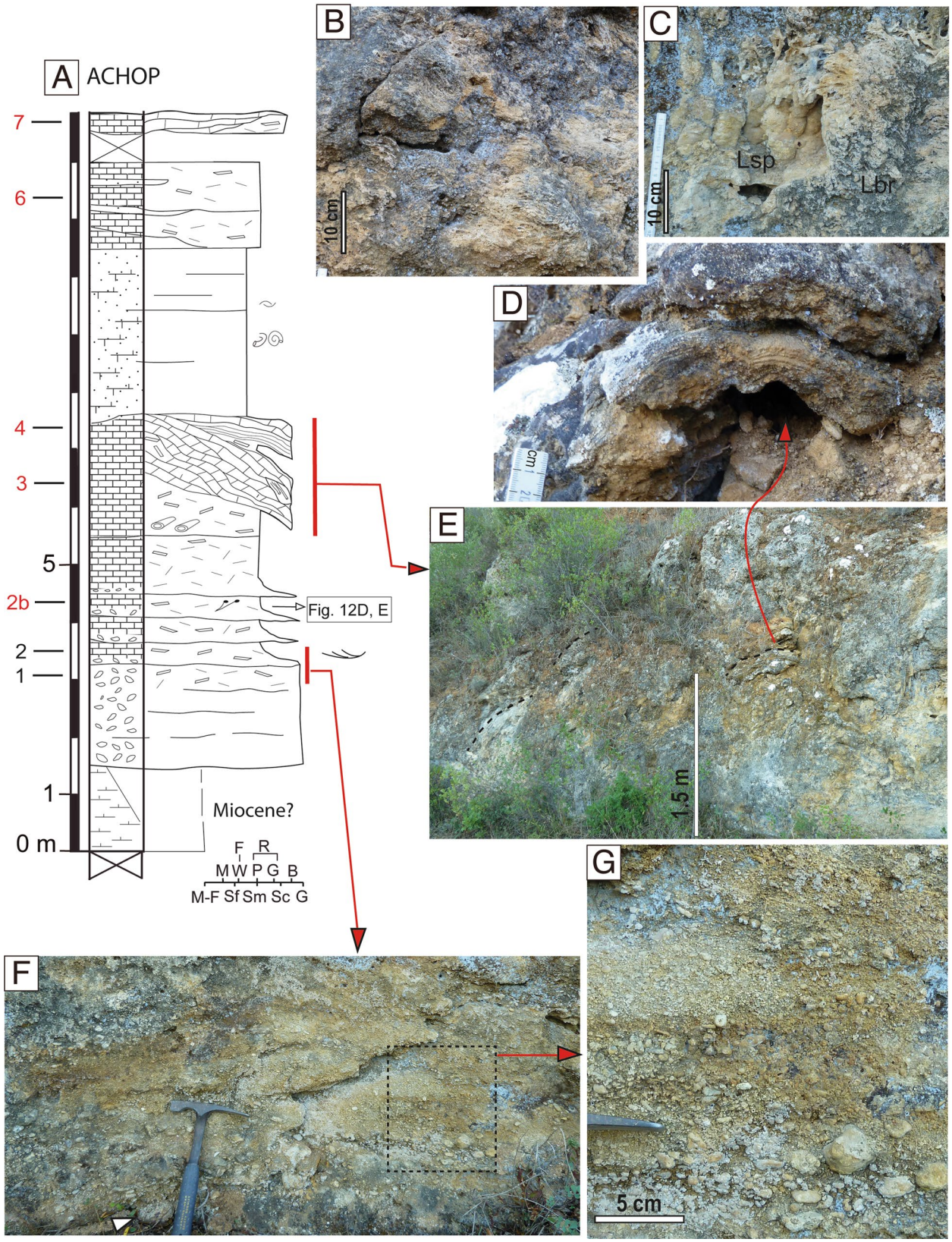
A ACHOP
7
6
4
3
5
2b
2
1
1
0 m
Miocene?
F R
M W P G B
M-F Sf Sm Sc G
Fig. 12D, E
B
10 cm
C
Lsp
Lbr
10 cm
D
E
1.5 m
F
G
5 cm

◂**Fig. 5** Stratigraphic section of Alto do Choupal (ACHOP) and related field images. The legend of symbols in **A** are given in Fig. 14B. **B** Boundstone consisting of inclined moss layers. **C** A small cavitiy with speleothemic overgrowth over down-growing stems (Lsp). On the right, vertical layer of moss boundstone Lbr). **D** Stromatolite dome. **E** Domed deposits consisting of highly inclined layers of moss boundstone, stromatolites and speleothems. Flow direction towards the left (southeast). **F** Phytoclast and minor oncoid rudstone (calcite coatings), including minor extraclasts. Note the oncoid to the left of hammer (arrow). **G** Detail of **F**, showing the fining-upwards evolution of the clast sizes

to the northwest of the Lapas terrace, is a 16 m-thick build-up composed of fine phytoclasts (Lphf), small oncoids and carbonate sands (Lo, Sb). Dating of a carbonate sand sample provided an age of 121.1 ± 14.7 ka (Fig. 2 and Table 1).

4.2.2 Pleistocene or Holocene deposits?

A small wedge-shaped deposit, which is 1.5–2 m thick, along a tributary of the Almonda valley (Vale Sobral; VSO, Figs. 2, 3) is mainly formed of stromatolite and speleothem laminated facies (Fig. 8A–C). It is tentatively set within MIS 5 due to its topographic position, but a different age could also be possible for the VSO.

At the Torres Novas locality, the MOICO build-up occurs on both banks of the present Almonda River (Figs. 2, 3). The MOICO section is 20.1 m thick and includes several nonexposed stretches (Fig. 9A). Close to the section's base, the lowermost tufa deposits in the sector almost reach the course of the present river, adding approximately 2 m to the total thickness in the MOICO section. Figures 9 and 10 illustrate the outcrop.

Dating the MOICO build-up is not straightforward. The only available age is from a sample of the uppermost deposit over an erosional surface (Fig. 4F); sample TNMC 03 yielded 8.97 ka, which is early Holocene (Table 1). Another sample taken for AAR dating (TNMC 01, Table 1) that is ca. 2 m above the course of the present river (approximately equivalent to metres 4–6 of the MOICO section; Fig. 9A), has not given a reliable age. Thus, the MOICO deposit below the erosional surface can correspond to any age older than 8.97 ka.

Interestingly, the alluvial terrace in the lowest reach of the Almonda River at the confluence with the Tagus River is the Tagus youngest terrace identified by Martins et al. (2008) and Martins & Cunha (2009). Dating this Tagus alluvial terrace (named T6 by those authors) by Infrared Stimulated Luminiscence (IRSL) at Azinhaga allowed the deposition of this terrace to be estimated to between 32 and 62 ka, i.e., MIS 3 (Cunha et al., 2016). Terraces T5 + T6 are identified to be equivalent to previously mapped terrace Q4 (8–15 m thick) in geological sheet 27-C (Manuppella et al., 2006) (Fig. 2). Q4 deposits appear at a lower topographic position and are inset into the MOICO build-up. Poorly exposed siliciclastic mudstones and gravel deposits that occur at an approximate position between metres 8 and 12 of the MOICO section are attributed to terrace Q4 herein. If the above considerations are correct, the MOICO build-up below the erosional surface should be older than MIS 3. The climate during MIS 4 was not favourable for tufa formation, as shown by the rare tufa record of most pair-numbered MISs (Martín Algarra et al, 2003; Sancho et al., 2015). Thus, an age within MIS 5 is tentatively proposed for the MOICO build-up, coinciding with the majority of deposits in the study area.

The uppermost deposits of the MOICO build-up, separated from the phytohermal bodies below through an erosional surface, are up to 1.5 m thick. These deposits consist mostly of phytoclast and intraclast rudstones with carbonate sand patches (where sample TNMC-3 was taken) and are poorly exposed and laterally discontinuous (Figs. 4F, 10E, F). The AAR dating placed them within the early Holocene (8.97 ka, Table 1). However, this age is not consistent with the high elevation of the deposits over the likely MIS-5 MOICO deposits. Moreover, the fact that the sample was taken from mixed-up sediments close to a human-made wall suggests that caution should be taken when considering the Holocene date. It is possible that the MOICO's uppermost deposits are closer in time to the underlying MOICO deposits.

The MPAU build-up crops out along the middle stretch on the right bank of the present Almonda River (Figs. 2, 3). The base is not observable; the outcropping deposits are 23 m thick. The top forms flat surfaces that at present are used for agricultural activities. The outcropping deposits are dominated by carbonate sands and silts, followed by stem boundstones and phytoclast rudstones (Figs. 4C, 11). The geomorphological and topographic positions of the MPAU build-up suggest that this deposit should have formed at the same time as others of the same elevation, as is the case for the LPCM, dated at MIS 5 (Table 1) and LAP deposits (Figs. 2, 3). Therefore, the MPAU build-up is tentatively set within the Pleistocene group, perhaps within MIS 5.

4.3 Sedimentology

4.3.1 Sedimentary facies

The sedimentary facies (i.e., lithofacies, as defined on the basis of the lithology and physical and biological features) present in the study area are diverse and have been described in other fluvial tufa-bearing systems (e.g., Arenas et al., 2000; Arenas-Abad et al., 2010; Azennoud et al., 2021; Capezzuoli et al., 2009; Ordóñez et al., 2016; Pedley, 1990, 2009; Rodríguez-Berriguete et al., 2018, 2021; Sallam, 2022; Vázquez-Urbez

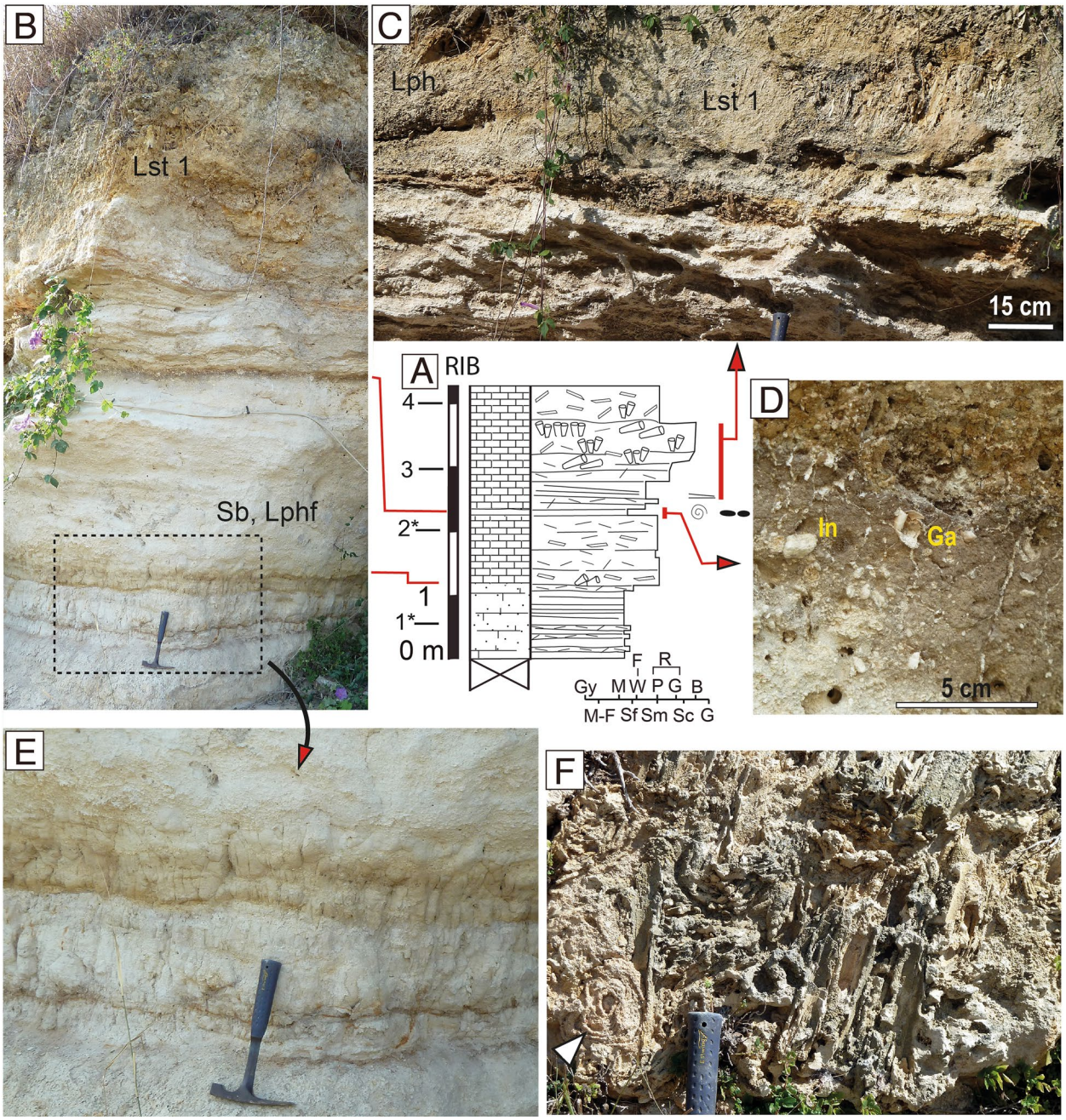

Fig. 6 Stratigraphic section of Ribeira Branca (RIB) and related field images. The legend of symbols in **A** are given in Fig. 14B. **B** Field view of the section, with dominant carbonate sand (Sb) and fine phytoclasts (Lphf), followed by facies Lst 1. **C** Downstream-inclined layers consisting of phytoclast and fine phystoclast rudstone, followed by fences formed of up-growing stem boundstone (Lst 1). **D** Lime mud and silt containing intraclasts (In) and gastropods (Ga). **E** Detail of B showing interbedded brown-coloured lime silts. **F** Detail of up-growing stem boundstone and some low-lying horizontal phytoclasts. Note the laminated calcite coatings (arrow). As per the inner diameter, the stems could correspond to cane-like vegetation

et al., 2012; Violante et al., 1994, among others). Herein, there is no distinctive difference between facies characteristics in the different build-ups; thus, no separation has been made when describing the facies. The dominant sedimentary facies are those consisting of carbonate sediments, followed by minor conglomerates and gravels. An array of carbonate facies has been distinguished based on geometry, textural features, sedimentary structures and biotic components (Table 4). The main mineralogy of all carbonate facies is calcite, as determined through microscopy analyses (both in optical and electron microscopy). The most abundant facies are the phytoclastic rudstones (Lph and Lphf), carbonate sands and silts with

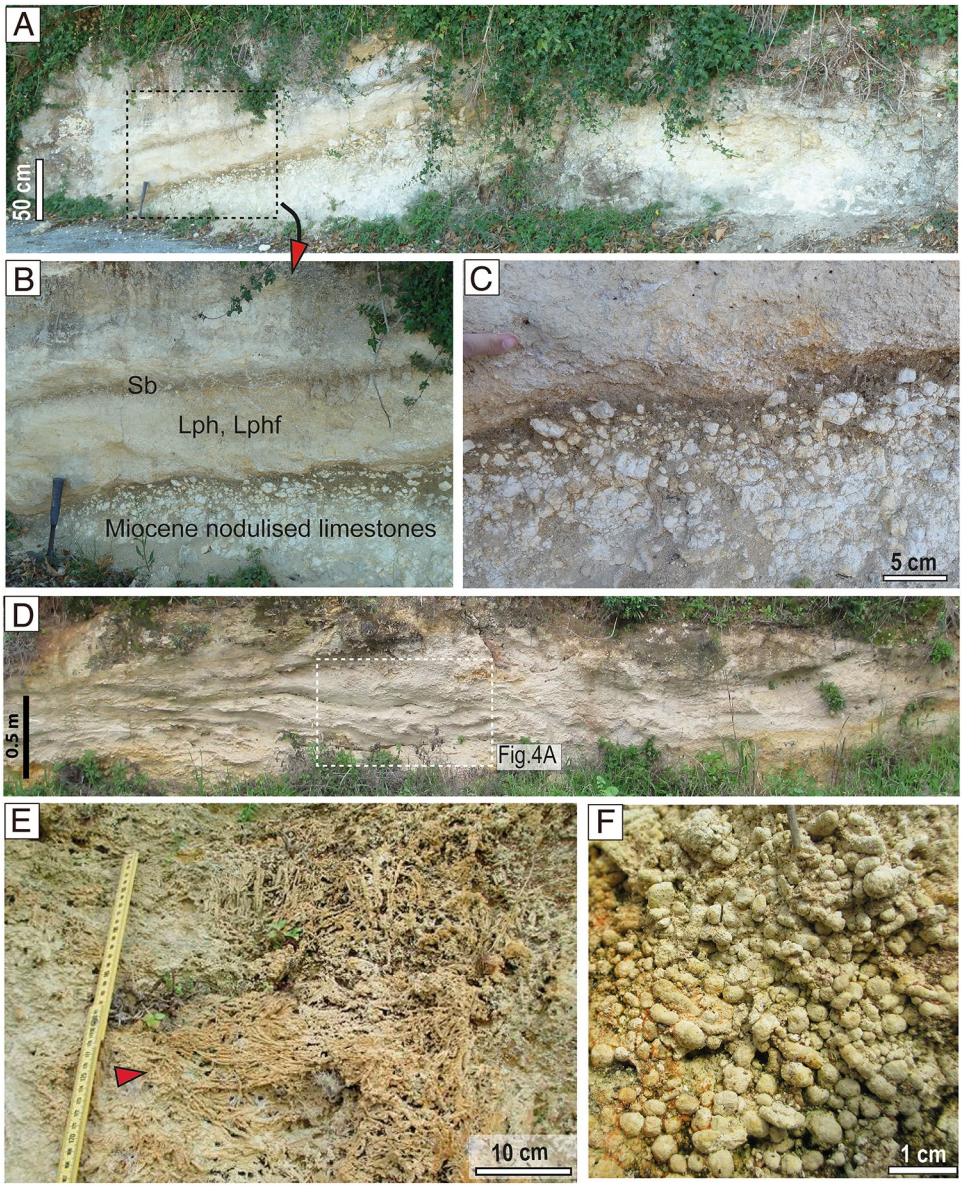

Fig. 7 Field images of Ribeira Branca (RIB), Ribeira Ruiva (RIBR) and Lapas (LAP) outcrops. **A** East–west-oriented outcrop showing fine phytoclast and phytoclast rudstone (Lph and Lphf), and carbonate sand layers (Sb) containing disperse extraclasts (Quaternary) over nodulised marly limestones (Miocene), close to the Ribeira Branca section. **B** and **C** Detailed images of A. **D** South–north-oriented outcrop consisting of stacked lenticular bodies formed of fine phytoclast and carbonate sand facies (Lphf and Sb) in the Riveira Ruiva build-up. **E** Charophyte-like, thin-stem bunches, partially lying in the horizontal position (arrow). Lapas build-up. **F** Small oncoids in a 0.4 m-thick deposit in the Lapas build-up

gastropods and ostracods (Sb) and stromatolites (Ls), followed by the moss boundstones (Lbr) and the up-growing stem boundstones (Lst 1). Less common are the down-growing stem boundstones (Lst 2), the oncolite rudstones (Lo) and the bioclastic and intraclastic limestones (Lb and Li). Speleothem facies (Lsp) are rare. A majority of calcite coatings on plant stems from either Lst 1, Lst 2 or Lph consist of several concentric laminae (Fig. 12A), which in most cases contain bacterial evidence, i.e., filamentous cyanobacterial calcite bodies arranged in fan- and bush-shaped bodies and isolated filaments (Fig. 12B, C). Cyanobacterial evidence is also found in stromatolites, oncolites and certain laminated speleothem deposits (Fig. 13A-F). Calcified moss caudilia and filidia can also contain bacterial evidence (Fig. 13G, H). Table 4 summarizes the most important macroscopic and microscopic characteristics of every facies, as well as their abundance, the facies that are commonly related to each other and their depositional environment interpretation. With the exception of the curtains of hanging stems (Lst 2) and speleothems (Lsp), most of these carbonate facies could have developed in several (sub)environments. Figures 4, 5, 6, 7, 8, 9, 10 and 11 show diverse macroscopic features, and Figs. 12 and 13 show diverse microscopic features of the different facies; the images in these figures are referred to Table 4.

4.3.2 Facies associations (FA) and depositional environments

The facies recognized in the studied Almonda valley outcrops are arranged vertically forming simple facies

associations (FAs) or sequences that record the sedimentary processes that occurred in a particular sedimentation area over time. Four main FAs were recognized (Fig. 14A). These FAs represent cycles of variation in water flow conditions (hydrodynamics), water level and/or migration of active parts in the fluvial system (Arenas-Abad et al., 2010). The four FAs formed by deposition in active channel zones, either with free-flowing water (FAs 1 and 2) or with standing or sluggish flow in dammed areas (FAs 3, 4 and the uppermost part of 1). FA 4 could have also formed in the floodplain. These sequences can lack one or more features, resulting in several incomplete variants (e.g., sequence 1a in Fig. 14A).

4.3.2.1 FA 1: Barrage-cascade and dammed areas This association represents the formation of a barrage-cascade from phytoclast accumulation and phytoherm growth and a dammed area upstream. It begins by erosion and then massive filling of a channel, initially with gravel and phytoclasts (facies G), and then evolves to dominant phytoclasts (Lph) (Fig. 5F, G). Locally, fine phytoclasts along with fragments of charophytes (Lphf and Lb) accumulated in areas that were protected from strong currents (Fig. 12D, E). The accumulation of phytoclasts (calcite coated stems of different sizes) could create an irregular channel floor, with areas acting as barrages. The progressive accumulation of moss layers (Lbr) in these areas would enlarge the barrages and produce cascades (Figs. 5B, E, 9B). In some areas, extensive microbial mats (Ls) alternated with moss layers (Figs. 5D, 9C, D, 10B), denoting changes in flow conditions. The faster

Fig. 9 Stratigraphic section of Moinho da Cova (MOICO) and related field images. The legend of the symbols in **A** are shown in Fig. 14B. The locations of the TNMC samples for AAR are indicated. **B** Moss and stromatolite boundstone forming a dome structure. On the right, note a smaller dome over a trunk mould lying horizontally (arrow). **C** Moss and stromatolite layers forming tight domes. The flow is towards the right (northeast). Note below a small cave with a stromatolitic speleothem coating. **D** Detail of stromatolite lamination in **C**. **E** Up-growing calcite-coated stem boundstone and associated phytoclasts, located between metres 4 and 5 in the MOICO section

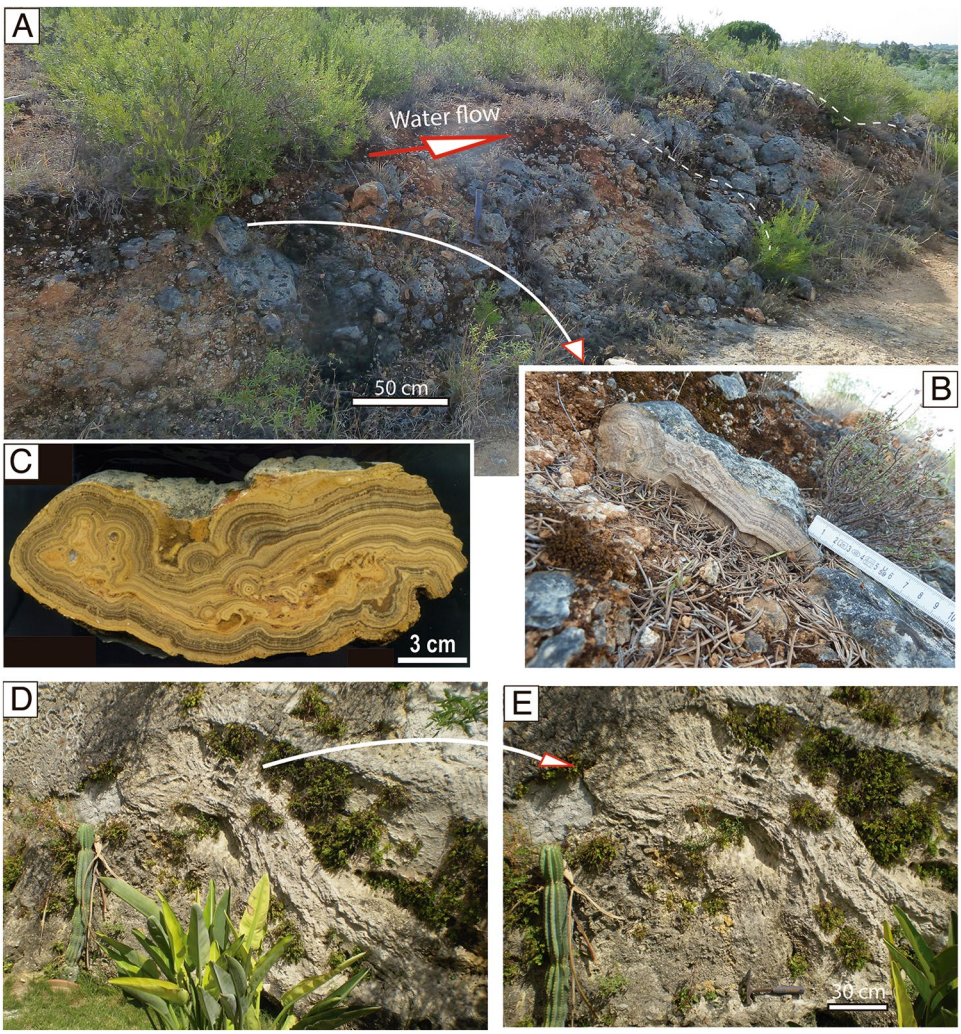

Fig. 8 **A**–**C** Field view and hand images of the Vale Sobral build-up (VSO). Note in A the inclined surfaces defined by laminated layers, both stromatolite (**B**) and speleothem (**C**). **D** and **E** Small domed deposit consisting of stromatolite and down-growing stems formed in a cascade at the downstream end of the Lapas build-up

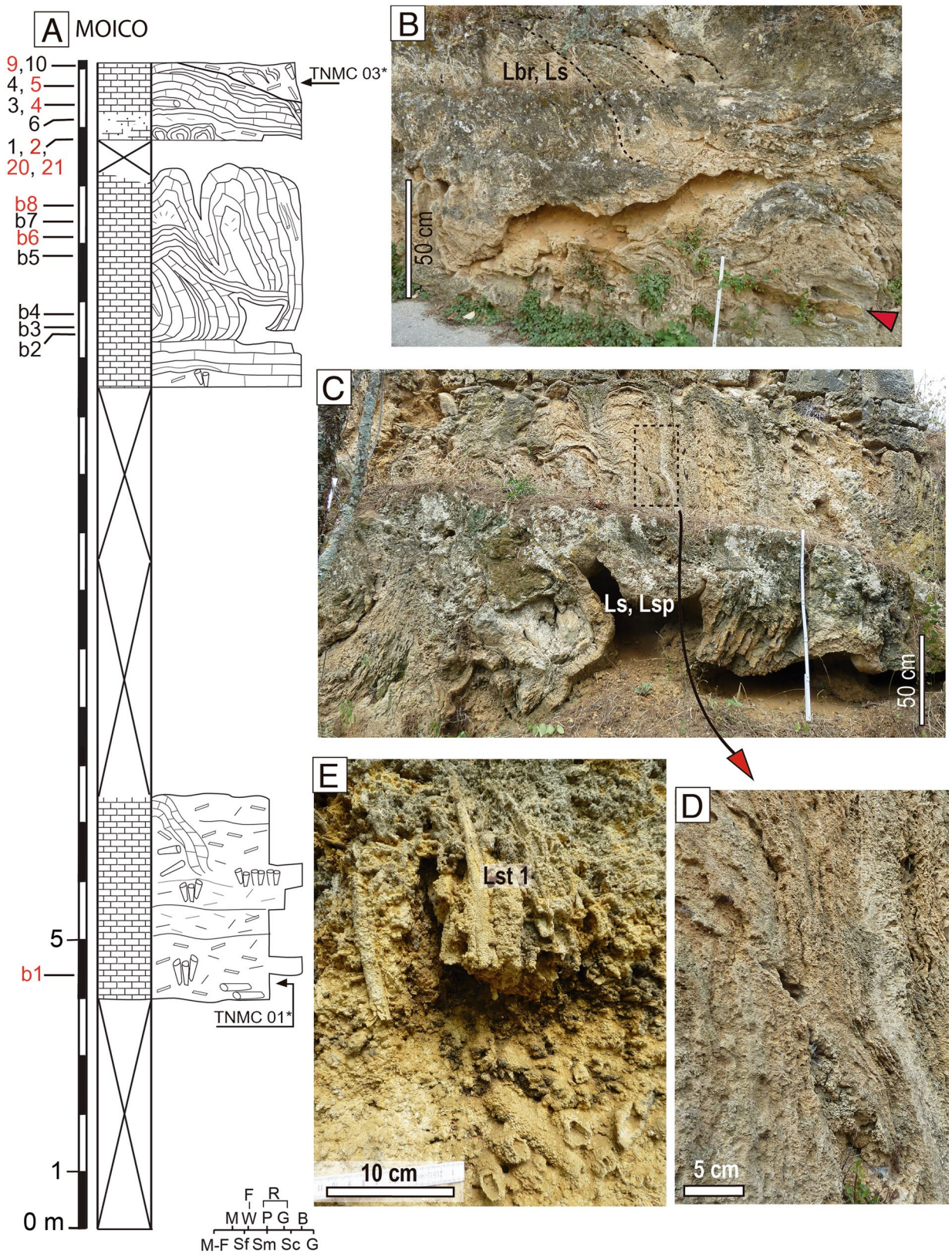
A MOICO
9,10
4, 5
3, 4
6
1, 2,
20, 21
b8
b7
b6
b5
b4
b3
b2
b1
5
1
0 m
TNMC 03*
TNMC 01*
F R
M W P G B
M-F Sf Sm Sc G
B
Lbr, Ls
50 cm
C
Ls, Lsp
50 cm
D
5 cm
E
Lst 1
10 cm

Table 4 Sedimentary facies: description of textural and structural features and depositional interpretation

Facies and abundance (Figures) Colour	Geometry of deposits	Microstructure, textural characteristics and components	Sedimentary structures	Identifiable biological content	Common associated facies	Depositional sedimentary context
Stromatolites. **Ls** ■■■ (Figs. 5B, 8, 9B, C, D, 10A–C) Beige and orange	Lenticular and domed deposits, with undulate base and top, 0.05 to 1 m thick. Metres in lateral extent	Laminated microbial boundstones (Figs. 10D, 12B, C, 13A). Undulate and irregular, alternating light (microspar) and dark (micrite) calcite laminae, up to 2 mm thick. Filamentous micrite bodies arranged as palisades and bush- and fan-shaped bodies, subperperdicular to lamination (Fig. 12B, C, 13B–E)	Flat and undulate lamination	Cyanobacteria and other bacteria	Lbr, Lst 2, Lsp and Lph	Stream stretches with irregular, at times highly inclined, floors (i.e., stepped cascades), over which water flows, commonly fast. Trapping micrite particles and bioinduced calcite precipitation forming microbial mats
Oncoidal limestones. **Lo** ■ (Figs. 5G, 7F) Beige to light grey	Commonly lenticular, up to 0.3 m thick, bodies, metres in lateral extent	Oncoid rudstones and rare packstones, commonly including phytoclasts and intraclasts. Oncoids are cylindrical and less abundant spherical in shape, up to 1.5 cm in diameter and 3 cm long. Nuclei mostly made of plant fragments. Calcite coatings up to a few mm thick made of light (spar and microspar) and dark (micrite) laminae, with abundant filamentous micrite bodies (Fig. 13F)	Structureless	Nuclei: fragments of coated macrophytes (higher plant stems and charophytes) Coatings: Microbial, mostly cyanobacterial, remains; insect traces	Lph, Lphf and Sb	Slow- to moderate-flowing, sometimes dammed, fluvial areas

Table 4 (continued)

Facies and abundance (Figures) Colour	Geometry of deposits	Microstructure, textural characteristics and components	Sedimentary structures	Identifiable biological content	Common associated facies	Depositional sedimentary context
Bioclastic limestones. **Lb** ■ Beige and light grey	Lenticular layers, 0.03 to 0.1 m thick, commonly associated with Sb and Lphf beds. Metres in lateral extent	Packstones and wackestones consisting of mostly floral remains, peloids and minor intraclasts. Less commonly, floatstones and mudstones. Lb may include gastropods and ostracods (entire and broken shells), charophyte portions and small oncoids (Fig. 12D) At places, mudstones to wackestones contain disperse calcite nodules mm to cm long	Structureless	Fragments of coated and calcified macrophytes (e.g., stems of charophytes)	Lph, Sb and Li	Aggradation in slow flowing and standing water areas along the channel (commonly dammed by barrages) and pools in the palustrine floodplain Accumulation of fine organic matter in stagnant water on the floodplain and in pools Drying out of mud sediment deposited in pools forming nodules. At places, the nodules are moved and mixed-up by currents Locally, currents may introduce sand- and silt-sized siliceous grains. Subaerial exposure and hardening by calcite and iron-rich cements
Bioclastic sands and silts. **Sb** ■■■ (Figs. 4A, C, E, 6B, E, D, 7B, D) Beige, white and light to dark grey	Tabular and lenticular beds (Fig.), up to 0.4 m thick, grouped in sets up to 2 m thick. Metres to decametres in lateral extent	Lime mud (mostly silt) and fine to coarse sand-size carbonate particles (mostly of flora). Poorly to slightly lithified. Sb may include gastropods, ostracods, oncoids, mm-long fragments of plant calcite coatings and intraclasts (Fig. 4B, D, 12F). Al places, lime mud layers include dark grey peaty laminae. Quartz and plagiocase angular grains are rare and sparse Locally, the beds containing siliciclastics are hardened by calcite and iron-rich cement	Structureless or with parallel lamination and banding. Gentle cross stratification Rare bioturbation by roots (Fig.) Nodules (Fig.)	Fragments of calcite-coated bryophytes and charophytes. Gastropods (entire and broken) and ostracods	Lphf, Lb and Li Lph	

Table 4 (continued)

Facies and abundance (Figures) Colour	Geometry of deposits	Microstructure, textural characteristics and components	Sedimentary structures	Identifiable biological content	Common associated facies	Depositional sedimentary context
Intraclastic and peloidal limestones. **Li** (■) (Figs. 4F, 10F) Beige to orange	Commonly, lenticular patches, rarely beds, up to a few cm thick, and metres in lateral extent	Packstones and rudstones consisting of massive micrite particles micrometer to mm long, mostly intraclasts and peloids, along with larger grains, such as stromatolite fragments and phytoclasts (Fig. 12G). In some cases, with ooids	Structureless	Unidentifiable	Lph, Lb and Sb	The same as above facies Lb, including breakage of semi-consolidated muddy intervals. Coarser texture deposits are associated with high-energy events that cause erosion over extensive surfaces and massive accumulation of heterogeneous carbonate sediments
Phytoclastic tufa. **Lph** ■■■■ (Figs. 5F, 6C, 11A, C) Very fine stems (mm long): **Lphf** Beige to orange	Tabular, undulate and lenticular beds and patches associated with Lst 1, up to 1.0 m thick. Decimeters to decametres wide	Macrophyte rudstones: non-organized, calcite coatings (outer casts) and external molds (imprints) of stems and other parts of plants, e.g., leaves; typically, plants are not preserved (decayed). Minor oncoids can be present. Inner imprints (rounded voids) up to 8 cm in diameter. Laminated coatings, up to 3 cm thick, around stems consisting of light (microspar) and dark (micrite) laminae with filamentous microbial bodies, arranged in palisades and adjacent bush-shaped bodies (Fig. 12A)	Structureless; in some cases, horizontal and undulate layering. Crude cross stratification in Lphf associated with Sb Rare groups of stems lying parallel to palaeoflow	Fragments and entire parts of macrophytes (trunks, stems, twigs and leaves). Gastropods	Lst 1 and Lbr Large phytoclasts can be associated with G Lphf associated with Sb	Breakage of stem phytoherm tufas and associated deposits (e.g., from palustrine zones) and uncoated plants. Debris (most of them already coated by calcite) are transported (short to long distances) and deposited close to formation areas, in floodplains and along active channels, at places forming barrage deposits. Fine phytoclasts (Lphf) accumulate mainly in dammed areas and floodplains
Phytoherm tufas consisting of:						
Stems. **Lst**:						

Table 4 (continued)

Facies and abundance (Figures) Colour	Geometry of deposits	Microstructure, textural characteristics and components	Sedimentary structures	Identifiable biological content	Common associated facies	Depositional sedimentary context
Bunches. Lst 1 ■■■ (Figs. 6C, F, 7E, 9E) Beige to orange	Lenticular bodies, commonly patches, 0.05 to 0.6 m thick, decimetres to metres in lateral extent; they form part of tabular and lenticular strata consisting of Lph, up to 0.5 m thick	Bunches and palisades of stems up to 0.6 m high. In some cases, boundstones of imprints. Vertical or subvertical stems of up-growing macrophytes are coated with laminated calcite, containing microbial evidence (Fig. 12C)		Portions of macrophytes (rushes, reeds and other grasses)	Lph and Lbr	Growth of hydrophilous vegetation and calcite precipitation in the submerged part of plants living in dammed areas upstream of barrages, flooded areas in the floodplain, and slow-flowing water areas and banks of some channels
Curtains. Lst 2 (■) (Fig. 8D, E) Beige to orange	Curtains, commonly just a few hanging stems, 0.8 m high and decimetres in lateral extent	Boundstones formed of hanging stems of down-growing macrophytes, highly inclined to vertical (90º); coated with laminated calcite		Hanging macrophytes (grasses)	Lph, Lbr and Lsp	Cascades in which hydrophilous hanging plants (groups of down-growing stems laying parallel to flow) are coated with calcite. Fast progradation of cascades fronts, occasionally forming overhangings
Bryophytes. Lbr ■■■ (Figs. 5E, 9B, C, 10A, B) Beige to orange	Hemi-domed and lenticular bodies (up to 2 m high), resulting mostly from stacking of moss layers. Metres to decametres wide	Boundstones consisting of moss layers (each 1.5–4 cm thick), in which caulidia and phyllidia become coated with calcite (Fig. 5B). Caulidia are parallel forming dense layers (Fig. 13G, H)	Banding formed from stacked moss layers (Figs)	Bryophytes (moss mats) and other minor macrophytes	Ls, Lph, Lst 1, Lst 2 and Lsp.	Cascades, jumps along the stream and barrage-cascades with preferential growth of moss mats that are coated with calcite In some bodies, Lbr layers alternate with Ls layers, denoting changing water flow conditions
Speleothems. **Lsp** (Fig. 5C, 9C) (■) Beige and orange	Variable shape and dimension. Up to 0.5 m high and a 1–2 m long	Calcite coatings on cave surfaces including stalactites. Laminated spar and micrite calcite, dense deposits. Lamination includes microbial micrite filaments (Fig. 8C, 13E)	Undulate lamination	Cyanobacteria and other bacteria	Lbr, Ls and Lst 2	Small caves, mostly developed below cascades with prograding upper fronts. Calcite precipitation on previously coated hanging stems and on other surfaces. Common stromatolite lamination

Table 4 (continued)

Facies and abundance (Figures) Colour	Geometry of deposits	Microstructure, textural characteristics and components	Sedimentary structures	Identifiable biological content	Common associated facies	Depositional sedimentary context
Conglomerates and gravels. **Gm** (Fig. 5F) ■ Beige and grey	Lenticular bodies, decimetres to 2 m thick	Clast supported. Varied nature of particles: Mesozoic and Miocene limestones, and minor siliceous particle rocks, up to 7 cm long. Sandy matrix and minor or absent carbonate cement. They form gravelly fining-upward sequences. Bodies of facies G fom thin layers at the base of lenticular bodies consisting of Lph	Structureless	Molds of trunks and calcite coatings of stems (Lph)	Lph	Gravel deposition in fluvial channels during high discharge events

■Occasional ■ Minor

■■Common

■■■Very common

■■■■Ubiquitous

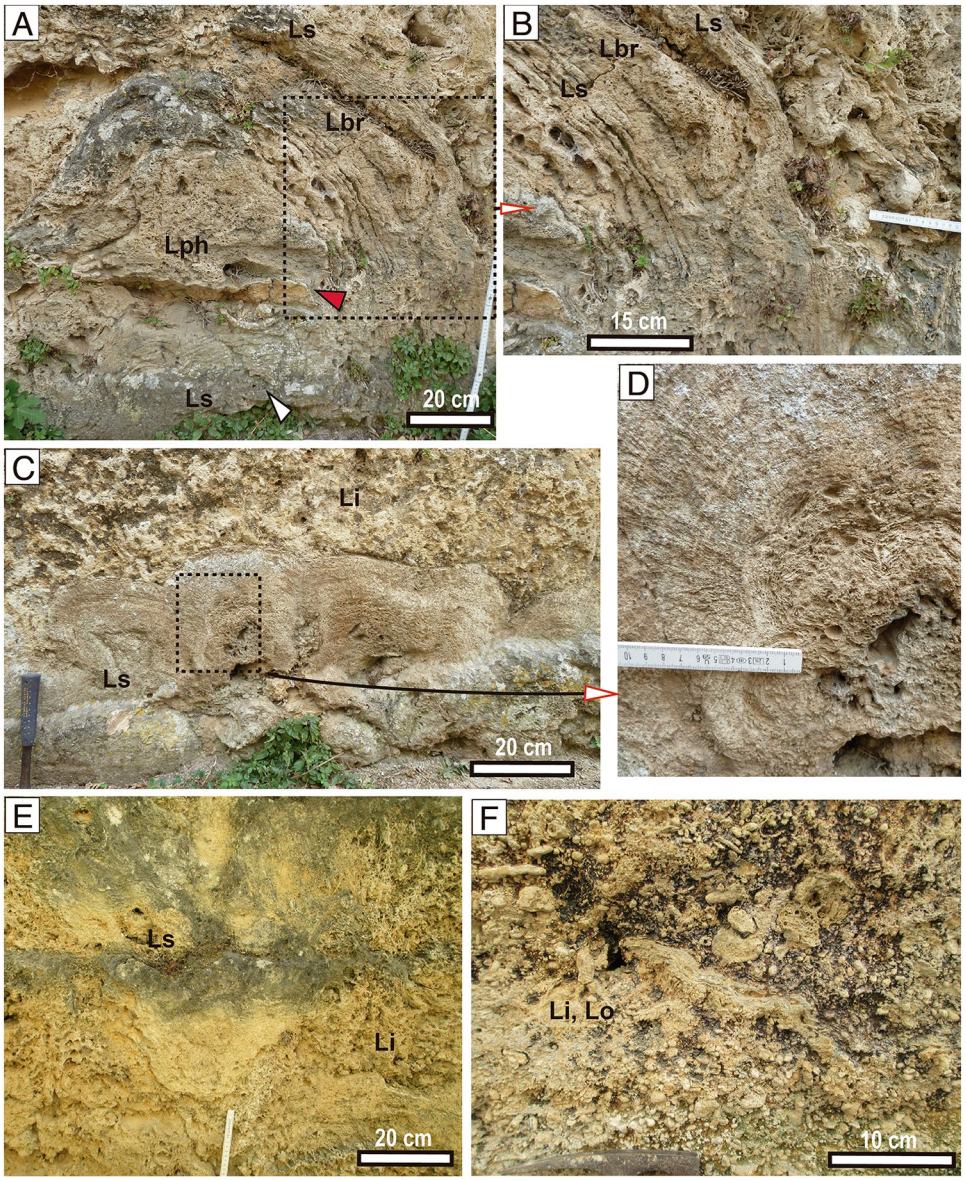

Fig. 10 Field images of the Moinho da Cova (MOICO) section **A**–**E** and close areas (**F**). **A** Dome consisting of moss and stromatolite layers that grew on phytoclast deposits, with a trunk mould lying horizontally (red arrow). The deposit below the trunk is also stromatolitic (white arrow). **B** Detail of A. **C** Stromatolite bed consisting of contiguous domed bodies underlying a chaotic deposit formed of intraclasts and phytoclasts that represent deposition after erosion. The stromatolite bed is partly eroded. **D** Detail of a domed body, with small phytoclasts in the nucleus. **E** Chaotic phytoclast and intraclast deposits of the upper part of the MOICO section. Note the channel-like surface with laminated deposits over it. **F** Phytoclast, intraclast and oncoid rudstone at the upper part of the MOICO build-up on the river's left bank

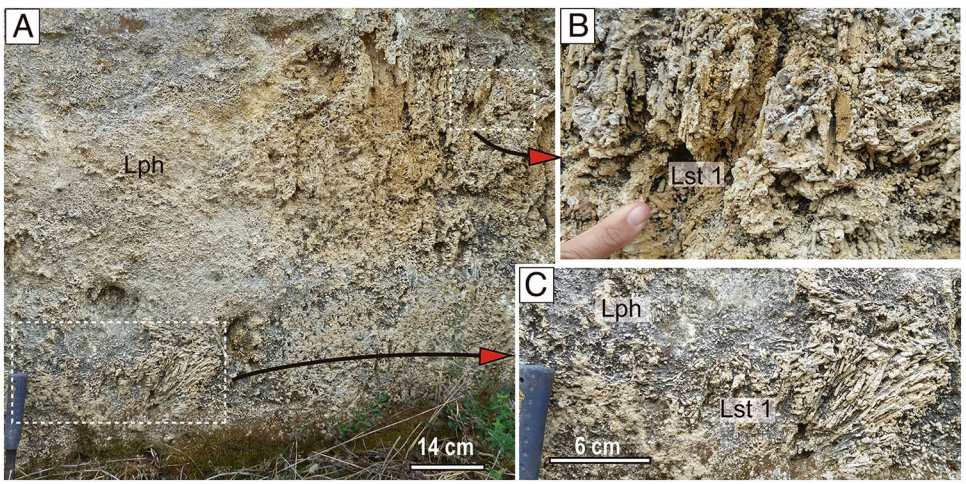

Fig. 11 Field views of deposits in the Moinho do Pau build-up (MPAU). **A** Phytoherms consisting of calcite-coated up-growing stems (facies Lst 1), laterally associated with calcite-coated phytoclasts (Lph). **B** and **C** Detailed images of facies Lst 1 and Lph shown in **A**

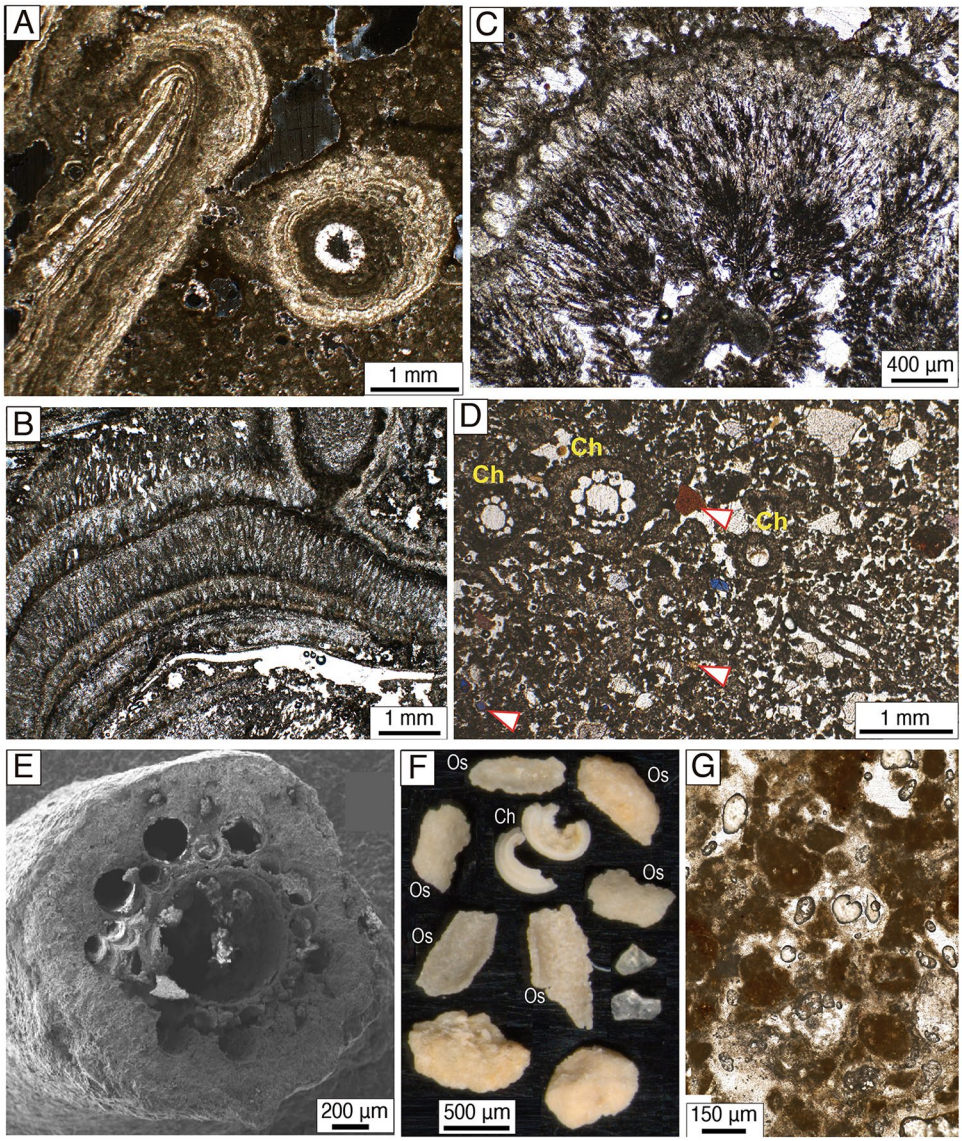

Fig. 12 Photomicrographs of tufa and associated facies (optical and SEM). **A** Phytoclast rudstone (Lph). Note the laminated spar and micritic calcite around the plant sections. MOICO section. **B** Stromatolite lamination (Ls) consisting of alternating thick light laminae and thin dark laminae. Light laminae contain micrite cyanobacterial filaments set perpendicular to lamination. Note at the base the empty mould of an insect. MOICO section. **C** Fan-shaped body developed in the laminated calcite coating of a trunk. Note the radially set structure corresponding to cyanobacterial filaments. MOICO section. **D** Packstone consisting of Charophyte stems (Ch) and intraclasts (Lb), with minor extraclasts (arrow). ACHOP section. **E** Cross-section of a Charophyte stem coated by calcite, of the same sample as D (SEM view). ACHOP section. **F** Fragmented ostracod and charophyte components in carbonate sand. ACHOP section. **G** Carbonate sand consisting of intraclast and peloidal ooidal grains (Sb). Lapas build-up

progradation of the cascade front, with respect to the foot, would create overhangs from which plants would hang and become coated by calcite (Lst 2). Below and behind these overhangs, small caves with speleothemic facies (Lsp) could form (Figs. 5C, 9C). Water pooled in areas upstream of the barrages were sites for lime mud and fine-sized bioclastic sediment accumulation, including skeletons of ostracods and gastropods living there (facies Sb, Lphf and Lb; Fig. 12F, G), as well as minor intraclasts and oncoids (Li and Lo). Charophyte stems and gyrogonites are preserved as fine particles in facies Sb and Lb (Fig. 12D). The shallow parts of these dammed areas could be colonized by hydrophilous plants, the submerged parts of which would be coated by calcite (facies Lst 1).

The ACHOP build-up contains a good example of the complete development of this association (Fig. 5). Variants of this FA comprise (1) the occurrence of cascades without damming water upstream, as in the case of VSO build-up (Fig. 8A), in which stromatolite and laminated speleothem deposits are dominant (Figs. 8B, 8C, 13E); (2) the lack of coarse detrital sediments at the base, as in the MOICO build-up; and (3) the lack of barrage-cascade formation (variant 1a, Fig. 14A). The latter denotes a lower slope, which favoured the development of bedforms (i.e., cross-stratification within fine phytoclasts) and the development of extensive pooled areas, where diverse biota could live and organic matter-rich intervals could form. Variant 1a is present in RIBR and close to the RIB buildp-up (Fig. 7A, B).

This sequence is typical of steep stretches associated with dammed areas in stepped fluvial systems and has been recognized in many Quaternary fluvial systems, e.g., in central Spain, the Lagunas de Ruidera (Ordóñez et al., 2005) and western Turkey (Töker, 2017), and described in several other Quaternary examples of southern Italy (Violante et al., 1994)

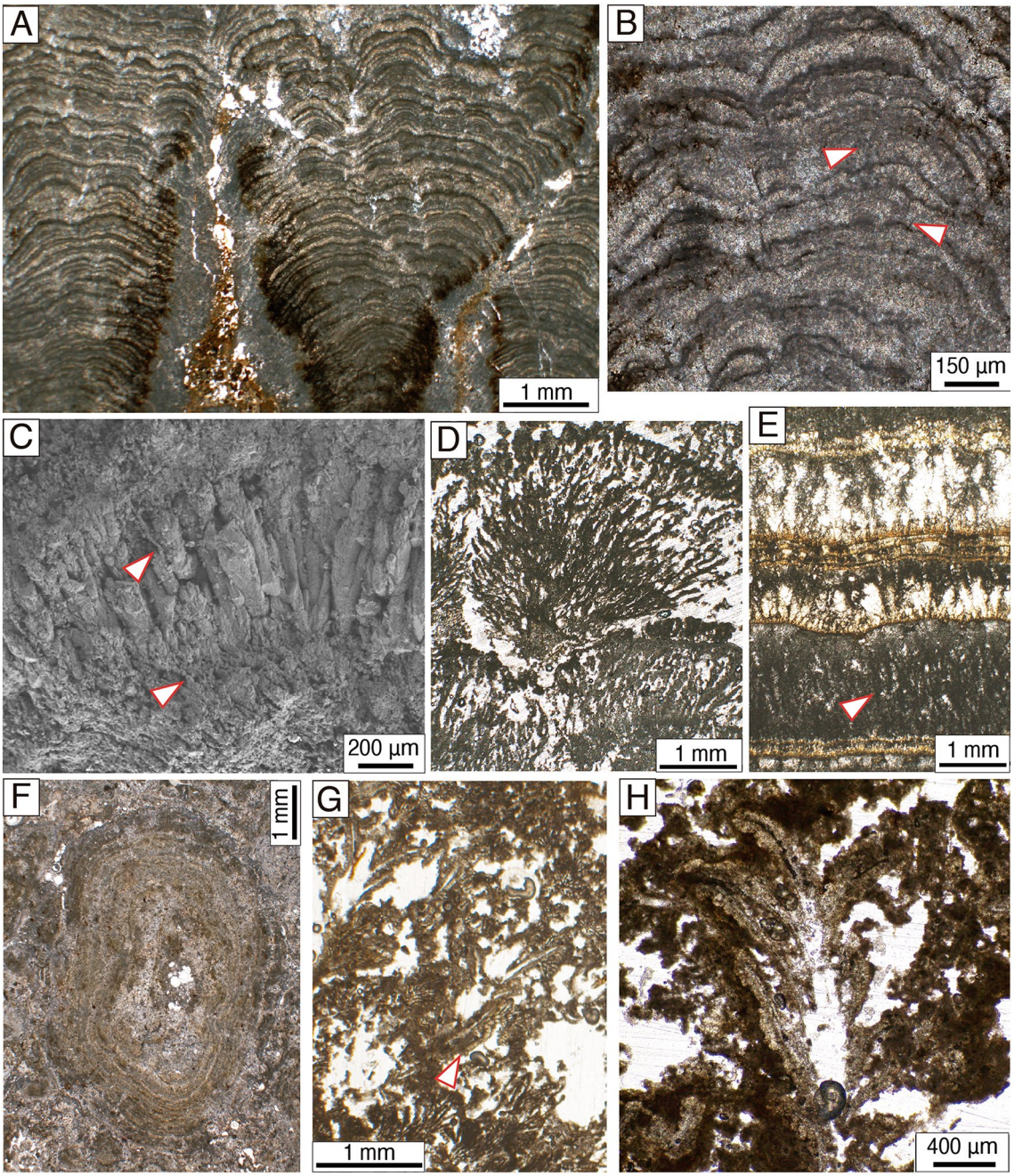

Fig. 13 Photomicrographs of tufa and associated facies (optical and SEM). **A** Columnar stromatolite (Ls) in a cascade build-up of the MOICO section. **B** Detail of lamination in A, showing alternating light spar and dark micrite laminae, both containing cyanobacterial filaments (arrow). **C** Stromatolite laminae (SEM). Note the different crystal size palisade and the presence of filaments (arrow). MOICO section. **D** Bush-shaped bodies consisting of cyanobacterial micrite filaments in a stromatolite. **E** Stromatolite lamination in a cascade of VSO. Note cyanobacterial filaments in micrite laminae (arrow) and crystal overgrowth in some thick laminae. VSO build-up. **F** Oncoid cross-section in a concoid rudstone of the LAP build-up. **G** Moss and cyanobacterial boundstone in a cascade of the MOICO build-up. Cyanobacterial filaments form palisades on moss and other biota (arrow). **H** Detail of moss caudilia mould in the MOICO build-up

and Spain (Arenas et al., 2014a; Arenas-Abad et al., 2010; Vázquez-Urbez et al., 2012).

4.3.2.2 FA 2: Low-slope channel This association illustrates deposition in gently sloped channel areas where hydrophilous plants could live in shallow water, producing facies Lst 1. Increased energy episodes caused breakage of the already calcite-coated plants, and fragments accumulated in close areas (Lph, Li; Fig. 12A, B, C). Small domes could form from moss layers coating the phytoclast accumulations, pro-

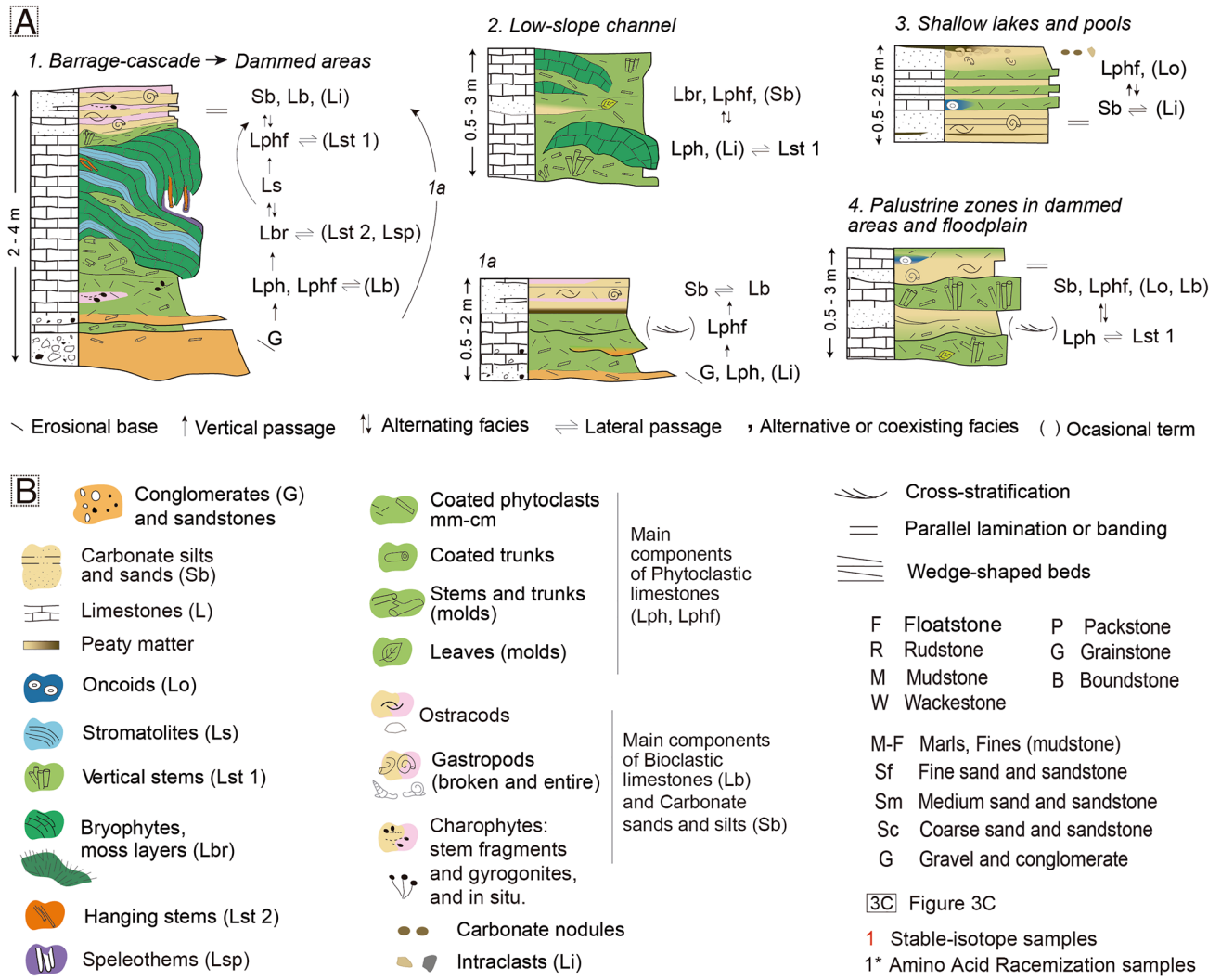

Fig. 14 **A** Vertical associations of sedimentary facies (FA). **B** Legend of symbols for **A** and Figs. 5, 6, 7, 8, 9, 10, 11 and 16

ducing facies Lbr. Water would be pooled upstream and/or between the domes; these small pools would be sites for the deposition of carbonate sand and silt (Sb), fine phytoclasts (Lphf) and rare intraclasts (Li). Aggradation would lead to the filling of these low-slope channel areas. This FA is common in the LAP build-up and the lower part of the MOICO build-up, e.g. metres 4–8 of the section (Fig. 9A, E).

Similar facies associations have been described in Quaternary deposits of southern Italy (Violante et al., 1994) and Holocene deposits in the Añamaza valley, N of Spain (Arenas et al., 2014a), representing areas of low-energy water flow conditions along the valley. The lack of stromatolites in the domes would imply more homogenous flow conditions than in the case described in Spain.

4.3.2.3 FA 3: Shallow lakes and pools Facies association 3 records deposition in shallow water areas of diverse extents. Typically, the most abundant facies were the bioclastic sands and silts (Sb) and less common intraclastic limestones (Li), which produced thick accumulations containing skeletons of ostracods and gastropods (Fig. 6B, D). Carbonate particles were derived from the breakage of upstream tufa and in situ calcite precipitation (lime mud) (Fig. 12F, G). Locally, some thin layers (i.e., 1–2 cm thick) contain microscopic organic matter, suggesting standing water conditions (Fig. 7B). Fine phytoclasts were introduced during slightly more agitated conditions, from the breakage of thin phytoclasts in littoral zones. These inputs were episodic and gave rise to cm-thick layering consisting of alternating Sb and Lphf facies, with less common millimetre- to 2-cm long oncoids (Lo; Fig. 7F). Filling and desiccation produced nodules and, in some cases, in situ intraclasts (breccia).

This association is well developed in the middle stretch of the Almonda valley, e.g., LAP, RIB and RIBR build-ups (Figs. 6A, B, D, E, 7A, B). Similar facies associations have been recognized in Quaternary deposits of southern Italy (Buccino et al., 1978), in Holocene deposits of the Lagunas de Ruidera (Ordóñez et al., 2005) and in Holocene deposits of the Añamaza valley (Arenas et al., 2014a), in the central and northeast Iberian Peninsula.

4.3.2.4 FA 4: Palustrine zones in dammed areas and floodplains Facies association 4 was produced in flat zones of the valley with a dense cover of hydrophilous vegetation, including dammed areas along the channel and in the floodplain. The submerged parts of plants would be coated by calcite, producing extensive blankets of facies Lst 1 (Figs. 6C, 11A). Disruption by gentle water currents and accumulation of fragments in close areas would form facies Lph and minor oncoids (Lo). These vegetated areas could be flooded as a result of water flow increases during rainy seasons and/or aggradation of downstream barrages, as described in Holocene deposits of the Añamaza valley (Arenas et al., 2014a). Typical facies resulting from these flooding conditions are Sb, Lphf and Lb. Erosive concave-up surfaces and cross-stratification in facies Lphf denote periods of increased water inputs.

This FA is very common in the record studied herein. The RIB, LAP and MPAU buildp-ups show good examples of extensive palustrine zones (Figs. 6A, C, F, 11). Similar associations that formed in extensive palustrine zones are common in many low-slope river stretches and have been described in association with both fluvial and fluvial–lacustrine environments in the Mediterranean realm (Ajuaba et al., 2021; Arenas et al., 2014a; Henchiri, 2014; Pedley et al., 2003; Vázquez-Urbez et al., 2012) and in southern Portugal (Guerreiro, 2015).

4.3.3 Sedimentological characteristics of some build-ups

The geometry of the build-ups is not always evident due to the present vegetation cover and anthropic activities. In a few cases, wedge-shaped bodies consisting of moss boundstones (Lbr) and stromatolites (Ls) with increasing thickness downstream are observable, although these bodies represent partial development of larger structures (e.g., at VSO and ACHOP) (Figs. 5A, 8A).

It is worth highlighting the extensive areas occupied by some fine-grained carbonate and stem phytoherm deposits in the middle stretch of the Almonda River valley. These consist of a dominance of phytoclast rudstones and boundstones (Lph, Lphf, and Lst 1) and carbonate sands and silts (Sb). This is the case for the RIBR and RIB zones (Figs. 2, 6, 7) and many deposits in the Lapas locality (Figs. 2, 4E).

4.3.3.1 Upstream deposits The ACHOP and RIBR build-ups (13 and 22 m thick, respectively) contain gravel and conglomerate deposits at the base. The overlying carbonate deposits in ACHOP consist of alternating beds formed of moss boundstones and stromatolites (Lbr and Ls) and fine-grained carbonate deposits, i.e., phytoclast rudstones and boundstones (Lphf, Lst 1) and carbonate sand and silt (Sb) (Fig. 5), conforming to FA 1. The overlying carbonate deposits in the RIBR build-up contain stacked, decimetre-thick and metre to decametre-long lenticular bodies formed of facies Lphf and Sb, at places displaying cross-stratification (Figs. 4A, 7D), as expressed by FA 1a and 4.

4.3.3.2 Moinho do Pau deposits This build-up reaches 23 m thick (Fig. 2 show the location). The outcropping deposits are rather tabular. At the base, these deposits consist of sands and silts (Sb), either massive or banded, which are overlaid by dominant phytoclast rudstones (Lph) and laterally continuous up-growing stem boundstones (Ls 1) (Figs. 4C, 11). These deposits formed via lime mud and sand deposition in wide dammed areas, which later became colonized by dense covers of hydrophilous plants, the submerged parts of which were coated by calcite. This palustrine zone was subject to low-energy flooding processes and/or crossed by draining channels, which caused the breaking of already calcite-coated stems; the fragments accumulated without much transport, almost on-site. Depositional conditions for this build-up are represented by FA 4.

4.3.3.3 Lapas deposits This extensive build-up that reaches 16 m thick, stands out because of the tabular to lenticular geometry consisting mainly of an abundance of fine-grained carbonate deposits (i.e., Sb, Lphf), which are at places banded and laminated and showing depositional inclination. These deposits are associated with phytoclast rudstones and stem boundstones (Lph, Lst 1; Fig. 7E) and less common 20- to 50 cm thick layers consisting of small oncoids (Lo; Fig. 7F). At places, horizontal-lying thin-stem bunches that appear visually similar to charophytes mark the flow directions (Fig. 7E). These deposits formed in large dammed areas, with slow flowing water and bearing palustrine vegetation (e.g., as represented by FA 3 and 4). Moreover, at the downstream end of the Lapas build-up, highly inclined moss and stromatolite layers (Lbr and Ls) and down-growing calcite-coated stems (Lst 2), that together form hemidomic bodies (Fig. 8D, E), reflect deposition in a small cascade that could have dammed water upstream, allowing the thick and extensive deposition of fine-grained deposits (i.e., conforming to FA 1 or 2).

4.3.3.4 Moinho da Cova deposits The lowermost outcropping portion consists of phytoclastic rudstones and boundstones (Lph and Lst 1; Fig. 9E) that constitute extensive

tabular layers, associated with small domes formed of bryophyte boundstones (Lbr), which produce inclined lenticular beds, i.e., as in FA 2. This portion of the build-up represents deposition in flat areas with abundant palustrine zones. On the southern bank of the present river, equivalent layers are dominated by phytoclast and intraclast tabular beds (Lph and Li) (Fig. 10F), indicating dominant breakage processes by currents.

The upper outcropping portion is dominated by thick and extensive bryophyte boundstones and stromatolites (Lbr and Ls), most of which form highly inclined lenticular or prism-shaped beds, with interbedded lenses consisting of calcite-coated hanging plants, Lst 2 (Fig. 9B, C). These facies corresponded to cascades or barrage-cascades structures (e.g., as in FA 1) that were at least of 2 m high and would grow across an extensive area of the river. This was a steep part of the valley that was broad enough to allow wide cascades and variations in the main channel direction. The main water direction in this deposit was northwards.

An erosional surface separates these phytohermal bodies from the uppermost deposits, which are up to 1.5 m thick. These deposits consist of phytoclast and intraclast limestones and carbonate sand patches that together form a discontinuous and rather chaotic deposit (Fig. 4F; 10E). These characteristics reflect deposition after a high-energy flow episode, which would have eroded the previous deposits, as reflected by the lower half of FA 1a.

4.4 Stable isotope composition

The studied tufa$\delta^{13}C$ values range from − 7.97 to − 10.84 ‰ V-PDB, and the $\delta^{18}O$ values range from − 4.07 to − 5.27 ‰ V-PDB, with mean values of − 10.11 and − 4.54 ‰ V-PDB, respectively (Table 4). These values are typical of meteoric fresh water with $^{12}CO_2$ influence (e.g., Andrews, 2006; Deocampo, 2010; Faure, 1998; Leng & Marshall, 2004). Differences in $\delta^{13}C$ between the different facies are small, except for four samples corresponding to facies Lst 2, Ls and Lbr (Lsp), two in each of the two analysed sections, which yield less negative values. Differences in $\delta^{18}O$ between the different facies are smaller. In terms of the section, mean $\delta^{13}C$ and $\delta^{18}O$ values of all samples are more negative in the MOICO section than in the ACHOP section (Fig. 15).

5 Discussion

5.1 Proposal of a sedimentary facies model

Figure 16 presents a sedimentary facies model for the study area. The area is noticeable by the extensive development of facies formed in still and slow-flowing water in dammed areas located along the middle stretch of the Almonda valley, coinciding with the lowest river slope stretch at present. These dammed areas provided sites for the deposition of fine carbonate sediment (Sb, Lb and Lphf), small oncolite formation (Lo) and growth of hydrophilous plants whose submerged parts became coated by calcite in shallow areas (Lst 1). Breakage of the latter would produce facies Lph (FAs 3 and 4). Gently sloped channel stretches were also present between knickpoints, favouring the development of vegetated zones (Lst 1) and the formation of phytoclasts (Lph), small oncoids (Lo) and small mounds consisting of moss mats (Lbr), as reflected by FA 2.

Facies denoting the presence of knickpoints typically form highly to moderately inclined beds, i.e., moss boundstones and stromatolites that developed in cascades and barrage-cascades. Calcification of moss mats and cyanobacterial mats that grew on step surfaces under moderate- to fast-flowing water produced mounds formed by Lbr and Ls (FA 1). Progradation of these structures caused the formation of small caves below and behind the cascade front, with speleothem deposits. These facies occur in a few places in the Almonda valley, e.g. in the ACHOP build-up (Fig. 5E), at the downstream end of the Lapas build-up (e.g., Fig. 8D, E)) and at Torres Novas, e.g. the MOICO build-up (Fig. 3). The visible height of these structures reaches 3 m.

Presently, the overall slope of the Almonda River is very low (0.33%), but has several areas with higher slopes (Fig. 3). Immediately after the source, along 270 m, the

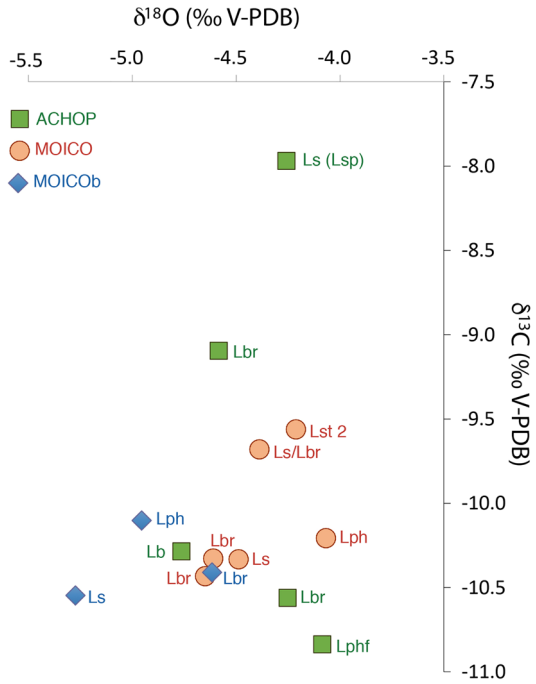

Fig. 15 Plot of stable isotope values ($\delta^{13}C$ versus $\delta^{18}O$, ‰ V-PDB). The corresponding facies are indicated for each case. Legend of symbols in Fig. 14B. See Table 3 for values

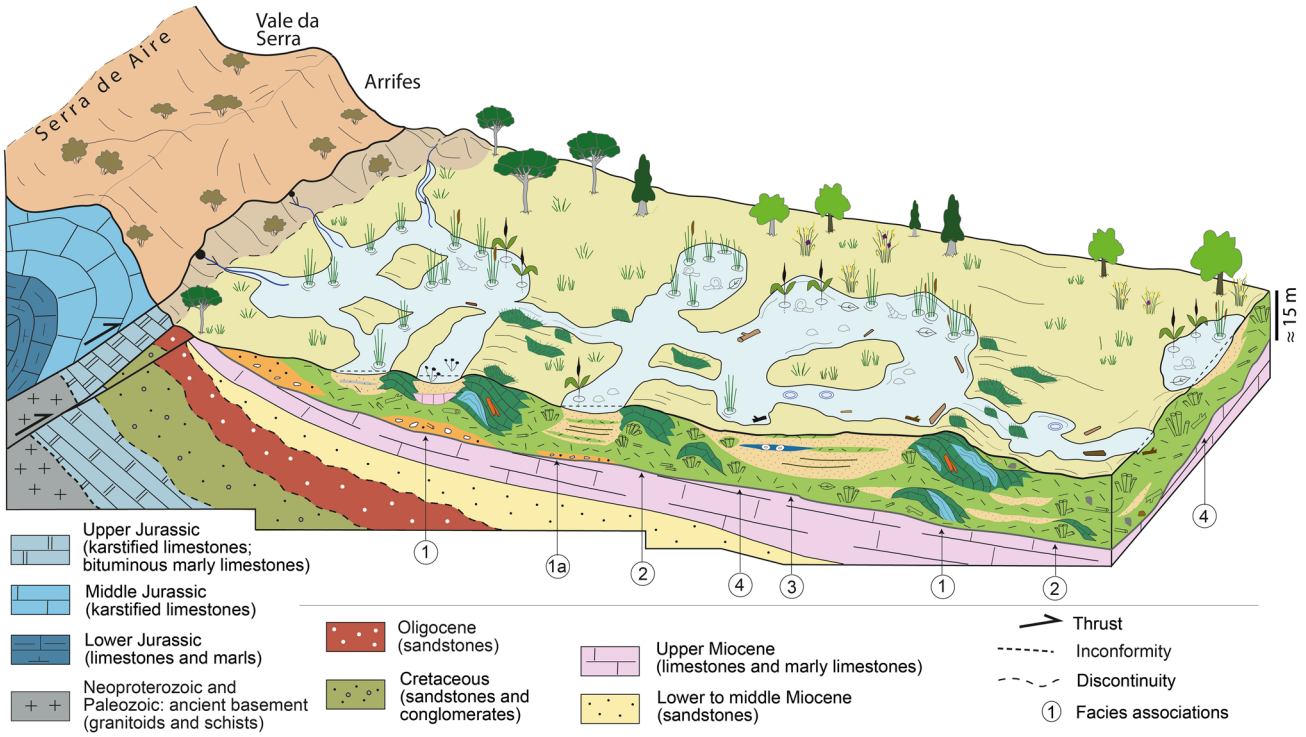

Fig. 16 Sedimentary facies model for the studied tufas and related deposits in the Almonda River valley. Legend of symbols in Fig. 14B

slope is steep (4%). After this point, the river floor shows several sections with an almost zero slope (0.00–0.03%), interspersed with sections with a slope of less than 1.5%, and the two steepest sections, with a 5.5% slope between Lapas and Torres Novas and a 4.6% slope in the Torres Novas locality (Fig. 3). The slope of the Quaternary Almonda valley was also small, as inferred from the position of the base of the tufa build-ups along the valley, the short height of the cascade-related structures and the large extent of deposits formed in dammed areas, which denotes a large separation between consecutive knickpoints. Therefore, the Quaternary tufas and allied sediments formed in a low- to moderately-sloped fluvial valley with a single watercourse and presented several short knickpoints and extensive flat areas between them. Local lateral tributaries were present in the upstream reach. This low- to moderately-sloped stepped fluvial system consisted of cascades, barrage-cascades and large slow-flowing and standing water areas. Palustrine conditions were present in the latter and in pools on the floodplain. Incision by channels occurred before or at the beginning of tufa deposition, as reflected by gravel and conglomerate deposits at the base of the several tufa build-ups (e.g., ACHOP and RIBR build-ups). Rare detrital deposits through some tufa sections denote later, much less intense and infrequent erosional processes. Overall, these erosional processes were related to episodes of increased precipitation that affected the Mesozoic and Cenozoic bedrock, causing higher water flow and providing the Pleistocene Almonda streams with gravels and intraclasts.

Despite the lack of clean outcrops along the flow direction, the carbonate facies distribution along the valley corresponds to a depositional architecture consisting of wedge-shaped bodies that thicken downstream (cf. Arenas et al., 2014a). Within each wedge-shaped body, the larger extent corresponds to facies Sb, Lph, Lphf, Lst 1 and Lo, which formed in low slope areas. In contrast, the downstream portion of the wedge-shaped bodies represents short spaces having facies that formed in moderate- to high-slope substrates, such as Ls, Lbr and Lst 2, which together produced the thickest deposits within a single wedge-shaped body.

This depositional arrangement is not different from the sedimentary facies models described for other stepped fluvial carbonate systems (Arenas et al., 2014a; Pedley, 2009; Vázquez-Urbez et al., 2012; Violante et al., 1994). Figure 16 presents a sketch that summarizes the most important features of the Pleistocene Almonda fluvial system. These features are as follows:

1) The first upstream tufa deposits occur approximately 2.5 km downstream of the Jurassic rocks; the main springs at present stem from the Jurassic rocks. This tufa occurrence coincides with the first upstream change in slope of the present river.

2) Gravel deposits occur mostly at the base of some tufa build-ups; these deposits formed in relation to high discharge events that provoked the erosion of previous rocks, incision into the Cenozoic bedrock and then deposition of polymict gravel (see Table 4).
3) Extensive deposits that formed in still and slow-flowing water areas occur in the middle stretch, between kilometres 5 and 8 of the valley, which at present corresponds to a very low slope area.
4) Palustrine conditions were extensive in association with large flat dammed areas and floodplains, at locations affected by currents that caused breaking of calcite-coated plants, with the resulting fragments accumulating very close to their origin.
5) Stromatolites occur in association with moss boundstones in moderate-to high-slope structures (stepped and vertical cascades), which represent short knickpoints along the river course.
6) The thickest outcropping deposits are in the downstream stretch, coinciding with relatively larger changes in slope.

5.2 Significance of the stable isotopic composition

The stable isotope values of the analysed samples are within the range of other fluvial tufas (mean $\delta^{13}C = -10.11‰$ V-PDB; mean $\delta^{18}O = -4.54‰$ V-PDB). The $\delta^{13}C$ values are typical of freshwater carbonates, and they are closer to the more negative extreme. The $\delta^{18}O$ values are biased towards the less negative extreme (Andrews, 2006; Faure, 1998).

Isotopic analyses of diverse groundwater points in the Almonda hydrographic basin yielded values between −3.5 and −5.3 ‰ for $\delta^{18}O$ and −18.7 and −30.1 for $\delta^{2}H$, with mean values of −4.6 and −24.5 ‰ V-SMOW (Antunes, 2016). Plotting of these values yielded a line that is close to the global meteoric line, thus indicating that the main recharge of the aquifer is precipitation, with negligible effects of altitude or continentality (Antunes, 2016).

The available $\delta^{18}O$ analyses of precipitation (rainfall) at several stations across Portugal (IAEA, 2005; Global Network of Isotopes in Precipitation-GNIP; https://www.iaea.org/services/networks/gnip; Carreira et al., 2009) can tentatively be compared with the groundwater $\delta^{18}O$ in the Almonda hydrographic basin. The altitude (maximum is 679 m; mean is 380 m) and mean precipitation (1200–1400 mm/year; https://www.ipma.pt/pt/educativa/tempo.clima/index.jsp?page=clima.pt.xml) of Serra de Aire are similar to those of Portalegre and Vila Real stations, with $\delta^{18}O$ values of −5.6 and −6 to 4 ‰ V-SMOW, respectively. The values of Portalegre and Vila Real stations are more negative than the −3.5 to −5.3 ‰ range of the groundwater in the Almonda basin. Assuming similar or slightly less negative $\delta^{18}O$ values for precipitation water in the Serra de Aire than in the Portalegre and Vila Real stations (due to its closer position to the coast), the difference may partially be due to the effects of residence time of water in the aquifer before water outflowing. A comparison with the Porto station would not be appropriate given the coastal position and low altitude, with $\delta^{18}O = -4.54$ ‰ V-SMOW.

The $\delta^{18}O$ values of the Almonda tufas (mean = −4.54‰ V-PDB, $N = 14$) are coherent with values of fluvial tufas formed in a temperate–climate zone, where there is sufficient throughflow for evaporation and residence time effects on river water to be considered negligible (cf. Andrews et al., 1997). Accordingly, the relatively high tufa $\delta^{18}O$ values may reflect an already ^{18}O-enriched river water, reflecting an initially ^{18}O-enriched water precipitation that is consistent with the proximity to the evaporation source and likely affected by the abovementioned residence time in the aquifer. Pertinent processes that may have amplified such enrichment in the fluvial environment are ^{16}O loss by flow agitation in turbulent areas, and fractionation effects due to temperature and calcite precipitation (Ortiz et al., 2006; Osácar et al., 2013).

The tufa $\delta^{18}O$ values in the Almonda valley are less negative than the values obtained in other fluvial deposits in central and NE Spain, both for Quaternary and recent tufas. For instance, in the Tagus River Basin, central Spain, Quaternary tufa deposits show mean $\delta^{18}O$ values of -6.72‰ V-PDB, $N = 74$ (Ortiz et al., 2009). In the Piedra River valley, NE Iberian Peninsula, the Quaternary mean $\delta^{18}O = -7.62‰$ V-PDB, N = 62 (Vázquez-Urbez et al., 2011), and recent tufa $\delta^{18}O$ values ranged from −7.13 to −9.28‰ V-PDB (Osácar et al., 2013). The recent water $\delta^{18}O$ values are less negative in the Almonda basin (−4.6 ‰ V-SMOW; Antunes, 2016) than in the Piedra River (-8.5 ‰ V-SMOW; Osácar et al., 2013). The latter difference may reflect the different ^{18}O depletion from the evaporation source to inland areas (*cf.* Faure, 1998).

Typically, the $\delta^{13}C$ values of the studied tufa (mean $\delta^{13}C = -10.11‰$ V-PDB, $N = 14$) reflect the input of soil-derived and/or organic matter-derived CO_2 in the water (Chafetz et al., 1991; Leng & Marshall, 2004). Two external sources of carbon could contribute to lowering the $\delta^{13}C$ of dissolved inorganic carbon (DIC) of water from which calcium carbonate would have precipitated: one is the dense vegetation cover on the catchment rocks and the other is the lithological composition of the aquifer rock (*cf*., Faure, 1998). It is worth highlighting the presence of bituminous shales in the Upper Jurassic sequence —described as "fetid bituminous marly limestones" by Manuppella et al., (2000, p. 65)— of the Estremenho Massif (Serra de Aire), which constitutes the catchment area. A long residence time of water in an aquifer can favour water enrichment in ^{12}C from both soil-derived and bituminous organic matter-derived CO_2. This ^{12}C signature would greatly counteract the ^{13}C

enrichment effects due to water being in contact with the aquifer marine carbonates.

The $\delta^{13}C$ values of the Almonda tufas are more negative than most Quaternary tufas in central and NE Spain. For instance, in the Tagus River Basin, central Spain, tufas show a mean $\delta^{13}C$ values of −7.10‰ V-PDB, $N=74$ (Ortiz et al., 2009), and in the NE of the Iberian Peninsula, the Piedra valley tufas have a mean $\delta^{13}C = -6.88$‰ V-PDB ($N=62$), and the Añamaza valley tufas have a mean $\delta^{13}C = -6.01$‰ V-PDB ($N=65$) (Vázquez-Urbez et al., 2011). This difference might be related to a series of factors concerning soil-derived CO_2, as tufa $\delta^{13}C$ values lower than −8‰ V-PDB usually indicate strong soil zone influence (Andrews et al., 1997). These factors include the characteristics of soils (e.g., thickness and type of soil vegetation) and the catchment rock composition and other basin-related features.

Apart from the production of plant- and soil-derived CO_2 within the tufa system as a result of the abundant plant cover, a series of intrinsic processes that influence the $\delta^{13}C$ of the DIC of fluvial water includes (Andrews, 2006; Pentecost & Spiro, 1990): (1) the preferential ^{12}CO uptake by plants; (2) the $^{12}CO_2$ output due to degassing, mainly in rapids and cascades, and (3) reaching an equilibrium between atmospheric and water CO_2. The three involve increasing $\delta^{13}C$ values in water DIC. The isotopic fractionation produces calcite $\delta^{13}C$ that is less negative than the water $\delta^{13}C$ from which it was precipitated (Faure, 1998; Osácar et al., 2013). Assessing the importance of each process and its imprint on calcite $\delta^{13}C$ is not a straightforward approach and usually involves complex experimental approaches (Arp et al., 2001, 2010).

In brief, water in the aquifer would have provided the outflowing Almonda River water with ^{12}C-rich and ^{18}O-rich CO_2, with the effects of further physical and biological processes of less importance on the stable isotope composition of tufa.

For the slightly more negative mean stable isotope values of MOICO compared to ACHOP samples, a speleothem sample in ACHOP greatly contributes to increasing the mean value. Except for that sample, the remaining values are similar. The increasing $\delta^{13}C$ values of the MOICO samples over time may reflect a decreasing input of ^{12}C in relation to the lesser development of soils, perhaps as a result of decreasing precipitation. These ideas must be taken as tentative given that a larger number of analysed samples would allow more conclusive results.

5.3 Factors influencing tufa formation

A wide array of factors can intervene in fluvial carbonate formation (Viles et al., 2007; Arenas-Abad et al., 2010; Della Porta, 2015; Arenas et al., 2014a; Capezzuoli et al., 2014; Toker, 2017; among others). Extrinsic factors include climate, tectonics, and bedrock composition and structure, including the characteristics of the aquifer feeding the fluvial systems. Intrinsic factors correspond to the presence of vegetation, physical and chemical properties of water and CO_2 degassing (Arenas-Abad et al., 2010). Moreover, some of these factors, i.e., temperature, may influence tufa formation on different scales, imprinting both cyclic and noncyclic climate signatures on the deposits.

The water composition of the Quaternary Almonda River had to be saturated in Ca^{+2} and HCO_3^- to form tufa calcite, a requirement that has been shown in studies of recent tufa-forming streams (Auqué et al., 2014; Kano et al., 2007; Kawai et al., 2006). Water coming from the Jurassic rock aquifer in the Serra de Aire provided such a required composition. The water composition of the present-day Almonda River supports such a statement (Antunes, 2016).

Moreover, as has been observed in recent streams, a certain distance from the spring is usually required for water pCO_2 loss to equilibrate with the pCO_2 atmosphere; then, pH increases and allows calcium carbonate to precipitate (Auqué et al., 2014; Chen et al., 2004; Liu et al., 1995). Calcite saturation levels increase downstream coinciding with the increase in the river slope, which enhances CO_2 loss, thus promoting rapid physico-chemical precipitation of calcite (Chen et al., 2004; Drysdale et al., 2002). In the Almonda case, the first tufa deposits along the main course occur approximately 2.5 km away from the present spring at the Jurassic/Cenozoic contact, which is a much shorter distance than in the Pleistocene tufa of the Piedra River (Arenas et al., 2014b).

Variations in water discharge can also influence the distance between springs and first tufa deposits (Arenas et al., 2014a; Drysdale et al., 2002). Accordingly, the comparatively short distance between tufa deposits and the Jurassic/Cenozoic contact might be indicative of moderate water discharge during deposition of the Pleistocene Almonda tufas. Nonetheless, studies of other tufas in nearby valleys would help discern this proposal.

5.3.1 Controls on the depositional architecture

Many present-day fluvial tufas are formed in streams that flow along valleys with variable slopes (Ford & Pedley, 1996; Pentecost, 2005). Tufas forming along stepped longitudinal profiles are the most common. In some cases, tufas develop as perched spring-line deposits on the valley sides and in very low slope areas within palustrine contexts (Arenas-Abad et al., 2010; Henchiri, 2014; Özkul et al., 2010; Pedley, 1990; Pedley et al., 2003). The studied tufa and allied deposits of the Almonda River valley formed in a stepped fluvial valley with a low to moderate slope.

Collectively, the different studies show that the geometry of the sedimentary fill mostly depends on extrinsic factors

that condition the topography of the basin floor, such as changes in bedrock composition and structure. Peña et al. (2000) and Toker (2017) described examples in which the presence of faults conditioned the floor topography and depositional fill geometry.

For the most part, abrupt changes in slope along the valley are related to changes in bedrock lithology, which offers different resistance to erosion (Arenas et al., 2014a; Vázquez-Urbez et al., 2012). These initial knickpoints favour the creation of cascades and rapids, on which tufa development is faster, due to the greater CO_2 loss in fast and turbulent flowing conditions (Violante et al., 1994; Pentecost, 2005; Kawai et al., 2006; Kano et al., 2007; Gradziński, 2010). Some areas in which trunks and calcite-coated plant debris accumulate are prone to produce cascades or barrage-cascades that pool water upstream. Faster deposition in all these areas with fast-flowing water tends to enlarge the initial knickpoints, resulting in the formation of a stepped longitudinal section with rapids, cascades, barrage-cascades, and still and slow-flowing dammed water areas (i.e., pools or lakes) (Arenas et al., 2014a).

As described above, the depositional geometry of the Pleistocene Almonda deposits corresponds to large, laterally related wedge-shaped bodies that thicken downstream, i.e., wedges with a large length/height (L/H) ratio formed in stretches with gentle slopes. In each wedge, a significant extent of deposits corresponds to the dammed facies and the other gentle-slope facies (i.e., fine-grained sediment, small oncoids, phytoclasts and up-growing calcite-coated stems). A much smaller extent corresponds to the high slope facies formed in moderate- to fast-flowing water (i.e., moss boundstones, stromatolites and down-growing stem boundstones).

The lack of large or high knickpoints and overall small to moderate slope of the Pleistocene Almonda River, with extensive gently sloped to flat areas corresponding to a large length/height (L/H) ratio, are likely related to 1) the absence of abrupt changes in the lithological composition of the bedrock, which is soft marls and limestones, and these rocks easily erodible, and 2) the bedrock structure, with a very small dip of the strata that the river crossed. The path of the Pleistocene Almonda River had almost perpendicular segments to the strike of the strata, which favoured small changes in slope when crossing rocks of different resistance. However, this situation was very different from other examples in which the bedrock consisted of lithological units with more contrasted resistance to erosion along the river path and with higher dip, causing higher knickpoints. This is the case for several Quaternary fluvial tufas in northeastern Spain (Arenas et al., 2014a; Vázquez-Urbez et al., 2012). Together these results show the strong control of bedrock composition and structure on the depositional architecture of fluvial carbonate deposits.

These results are consistent with other tufa studies. For instance, in the Pleistocene Ebrón River valley, NE of the Iberian Peninsula, the existence of a low sloped downstream stretch favoured the development of a dominant carbonate palustrine system (Ajuaba et al., 2021). There, the type of tufa facies and the depositional architecture clearly reflect the increase in width and decrease in slope of the sedimentary area as a result of the bedrock lithological and structural changes, from more resistant Mesozoic rocks upstream to less resistant Neogene detrital rocks with smaller dips downstream, together allowing a greater width and smaller slope of the sedimentary area downstream.

5.3.2 Climate and hydrology

Most tufa and allied deposits in the studied area herein appear to have formed during MIS 5 (likely MIS 5e and 5c; Gibbard et al., 2005). This stage was characterized by warm temperatures, which favoured the formation of important deposits of tufa in many high- and mid-latitude areas throughout the world, which are very abundant in the Mediterranean region (Durán, 1989; Martín Algarra et al., 2003; Pedley, 2009; Sancho et al., 2015). Precipitation seems to be a limiting factor in low-latitude regions and is more dependent on local to regional atmospheric conditions (Viles et al., 2007). The sensitivity of the Iberian Peninsula to shifts in the North Atlantic atmospheric belt makes any precipitation model more complex (Cacho et al., 2002). However, the proximity of the study area to the Atlantic humidity could favour the continuous recharge of the Mesozoic rock aquifer, thus assuring water availability during the formation of the studied tufas.

The outcropping studied record does not show evidence of vigorous erosion phases, except for the upper part of the MOICO build-up. This fact might be related to water flow regimes of little variation in intensity (i.e., with stable discharge), a characteristic that may be indicative of stable precipitation conditions, as occurs in temperate humid climate zones. Some studies have shown that highly variable flow regimes in arid and semiarid conditions can cause erosion phases and deposition of coarse clastic sediments that alternate with carbonate deposits (Viles et al., 2007), while rare flood-related deposits have been reported from tropical conditions in northern Australia (Carthew et al., 2003). Together, these facts suggest that the deposition of the Pleistocene Almonda tufas might have occurred under quite stable precipitation regimes, which allowed continuous water flow through the river and abundant hydrophilous plants to live in still and slow-flowing water zones.

6 Scientific interest and potential of tufas as natural, cultural and economic resources

This part of the text aims to highlight the importance of the use and preservation of tufas as natural, cultural and economic resources, considering the diverse scenarios in which tufas can stand out in a region: rock quarrying and building, water uses in agriculture, industry and urban areas, landscape, tourism, and cultural–educational activities. In addition to the vast scientific interest, the Almonda River valley is an extraordinary example to illustrate the management of tufa-depositing streams and their deposits as natural, cultural and economic resources in a region.

At present, some industrial and agricultural activities in the region are sourced with water derived from different points along the river, but primarily upstream. In the past, water mills ("moinhos") and dams were built in zones with slope changes. These anthropogenic elements indicate the type of tufa deposits and structures that developed along the river course in the past.

Some urban zones are built on tufa deposits, but tufa observation is possible, at least partially, from natural sections and open quarrying and long-cave digging. Paradoxically, the anthropogenic activity related to open-air tufa quarrying for building uses has provided numerous new outcrops that have broadened the available areas for diverse geological and paleontological studies. Several large, ancient open-air quarries are located in Moinho da Cova-Torres Novas, Alto do Choupal-Ribeira Ruiva, and Moinho do Pau-Lapas, some of which are more than 100 m long. There are a number of smaller quarries throughout the valley. Underground extraction of tufa has been accomplished by means of digging tunnels, which offer an opportunity to study the fluvial carbonate deposits of the Almonda River. Among the several examples, the extraordinarily complex net of tunnels excavated below the Lapas town that occupy most of the fluvial terrace stands out, spanning approximately 700 m of length, of which more than 400 m are opened to visitors (*Grutas de Lapas*). The age and origin of these tunnels are still unclear. Zbyszewski et al. (1974) referred to the existence of pre-historical caves in Ribeira Branca and Lapas. Santos and Reis (2021) considered the oldest items found in the tunnels could be atributed to a period between the Mesolithic and the Chalcolithic, within 8000–3000 years AC. However, the authors of the present contribution estimate that some natural, fluviokarstic tunnels may have formed during MIS 2–4.

Tufa extraction for building uses dates back to the medieval and ancient epochs, denoting the close relation between the geological resources and the cultural heritage of the region. This is the case for the Roman village *Cardilium* in Torres Novas. Many examples of public and private buildings using tufa as building material are also found throughout the Mediterranean zone.

As in the case of other tufa-depositing streams, the landscape along the Almonda River valley is spectacular, representing a touristic attraction. There are a number of paths with explanatory panels at significant points along the present river course. The sharp transition from the Estremenho massif to the Tagus Basin at Arrifes shows the karstic spring that feeds the Almonda River, stemming from the largest groundwater system in Portugal (*Gruta do Almonda*). This is a touristic attraction as well. One important and still pending point is the study of the present-day sedimentation process. The results can provide crucial information on tufa facies, deposition rates and hydrochemical composition, which can be used in future actions in the region and compared with other cases (e.g., the Piedra and Mesa Rivers in the NE Iberian Peninsula, and the Korana and Krka Rivers, in Croatia).

A great push toward tourism in the Almonda River region was achieved because of the geo-touristic requalification of the *Grutas de Lapas* by the *Torres Novas* municipality in 2018. A visitor centre with diverse information (geology, geography, history and archaeology) explains the varied tufa-related heritage in the region, underlying the geological significance (Fernandes, 2018). That action was awarded by ProGeo-Portugal.

The geological information offered in this paper hopes to raise the scientific interest in the tufas of this Portuguese region and elsewhere as tools for understanding the environmental, climatic and hydrological conditions of past scenarios. Moreover, the example of the Almonda valley tufas serves to emphasize that the correct management of present and ancient tufa-related contexts is crucial to value and preserve the varied tufa-related heritage.

7 Conclusions

The tufas and associated deposits of the Almonda River valley were deposited during the Middle-Late Pleistocene (MIS 5) in a low- to moderately sloped stepped fluvial system. It consisted of short barrages and barrage-cascades separated by large areas occupied by slow-flowing and still water. The latter were sites for diverse aquatic fauna and flora to live and for fine-grained sediment (carbonate sand, lime mud, fine phytoclasts, small oncoids and intraclasts) and up-growing stem boundstones to form. The moderate- to high-slope areas were sites for stromatolite, moss and down-growing stem boundstones to form. Incision by channels occurred before or at the beginning of tufa deposition. The homogeneous bedrock lithology and structure propitiated the small to moderate riverbed slope, which was later exaggerated by ongoing tufa growth at knickpoints.

Mostly stable precipitation regimes during the study tufa deposition are deduced from the lack of frequent and/

or intense erosional phases and the preservation of thick fine-grained sediments and palustrine facies.

Water springs stemming from the Jurassic rock aquifer provided water with sufficient Ca^{++} and HCO^{-}_{3} to reach calcite saturation levels a short distance downstream. The calcite $\delta^{13}C$ values of tufa facies reflect the influence of ^{12}C-rich CO_2 sourced by bituminous rocks and vegetation cover in the catchment area. The calcite $\delta^{18}O$ values suggest initially ^{18}O-rich CO_2 in the aquifer water, which was likely also affected by ^{18}O-enrichment due to residence time. The proximity of the study area to the Atlantic humid zone caused precipitation to be ^{16}O-depleted. Differences in calcite $\delta^{18}O$ composition with respect to Quaternary tufas in the central and eastern Iberian Peninsula support the differential ^{18}O depletion from the evaporation source to inland areas. The proximity also favoured the water recharge of the Mesozoic rock aquifer, assuring water availability during the formation of the studied tufas.

Acknowledgements This work forms part of the activities of the GeoTransfer scientific group (Aragón Government, Operating Program FEDER Aragón 2014-2022) and projects CG2009-09216BTE and CGL2013-42867-P of the Spanish Government and European Regional Funds. Funding was provided by these institutions. The scanning electron microscopy, optical microscopy and rock preparation services of the University of Zaragoza, Spain (*Servicios de Apoyo a la Investigación, SAI*), and the Stable Isotope Laboratory (*CCIT-UB Serveis*) of the University of Barcelona are thanked for technical support. The *Câmara Municipal of Torres Novas* facilitated technical and logistic support during the field campaigns. Mário Cachão, professor of Paleontology at the Science Faculty of the University of Lisbon, is greatly acknowledged by the first author for his enthusiasm to study this area and help during the initial stages of this work. The authors are grateful to Dr. Gonzalo Pardo and three anonymous reviewers, whose comments and suggestions helped improve the quality of the manuscript.

Funding Open Access funding provided thanks to the CRUE-CSIC agreement with Springer Nature.

Data availability All data and material supporting the research are available in the paper.

Declarations

Conflict of interest On behalf of all the authors, the corresponding author states that there is no conflict of interest.

References

Ajuaba, S., Arenas, C., & Capezzuoli, E. (2021). Sedimentology of Pleistocene palustrine tufas and associated deposits of the Ebrón Valley (Iberian Ranges, Spain). *Estudios Geológicos, 77*(1), e137. https://doi.org/10.3989/egeol.44131.593

Almeida, C., Mendonça, J. J. L., Jesus, M. R., & Gomes, A. J. (2000). *Sistemas aquíferos de Portugal Continental*. Sistema Nacional de Informação de Recursos Hídricos. http://snirh.pt/index.php?idMain=4&idItem=3&idISubtem=link1

Andrews, J. E. (2006). Palaeoclimatic records from stable isotopes in riverine tufas: Synthesis and review. *Earth-Sciences Reviews, 75*, 85–104.

Andrews, J. E., Riding, R., & Dennis, P. F. (1997). The stable isotope record of environmental and climatic signals in modern terrestrial microbial carbonates from Europe. *Palaeogeography, Palaeoclimatology, Palaeoecology, 129*, 171–189.

Antunes, A. L. G. (2016). *Caracterização Química e Isotópica das Águas Subterrâneas da Bacia Hidrográfica do Rio Almonda*. Mestrado em Geologia Aplicada, 78 p. Faculdade de Ciências, Departamento de Geologia, Universidade de Lisboa, Portugal.

Aranbarri, J., Sancho, C., Arenas, C., Bartolomé, M., Leunda, M., Rico, M. T., & González-Sampériz, P. (2021). Vegetation reconstruction related to Nogal de El Batán Holocene fluvial tufa buildup, Las Parras del Martín Iberian Range. *Cuaternario y Geomorfología, 35*(1–2), 49–68.

Arenas, C., Gutiérrez, F., Osácar, C., & Sancho, C. (2000). Sedimentology and geochemistry of fluvial-lacustrine tufa deposits controlled by evaporite solution subsidence in the central Ebro Depression, NE Spain. *Sedimentology, 47*, 883–909.

Arenas, C., Vázquez-Urbez, M., Auqué, L., Sancho, C., Osácar, C., & Pardo, G. (2014a). Intrinsic and extrinsic controls of spatial and temporal variations in modern fluvial tufa sedimentation: A thirteen-year record from a semiarid environment. *Sedimentology, 61*, 90–132.

Arenas, C., Vázquez-Urbez, M., Pardo, G., & Sancho, C. (2014b). Sedimentology and depositional architecture of tufas deposited in stepped fluvial systems of changing slope: Lessons from the Quaternary Añamaza valley (Iberian Range, Spain). *Sedimentology, 61*, 133–171.

Arenas-Abad, C., Vázquez-Urbez, M., Pardo-Tirapu, G., & Sancho-Marcén, C. (2010). Fluvial and associated carbonate deposits. In A. M. Alonso-Zarza & L. H. Tanner (Eds.), *Carbonates in continental settings* (pp. 133–175). Elsevier.

Arp, G., Bissett, A., Brinkmann, N., Cousin, S., De Beer, D., Friedl, T., Mohr, K. I., Neu, T. R., Reimer, A., Shiraishi, F., Stackebrandt, E., & Zippel, B. (2010). Tufa-forming biofilms of German karstwater streams: Microorganisms, exopolymers, hydrochemistry and calcification. In H. M. Pedley & M. Rogerson (Eds.), *Tufas and Speleothems: Unravelling the Microbial and Physical Controls* (Vol. 336, pp. 83–118). Geological Society, Special publications.

Arp, G., Wedemeyer, N., & Reitner, J. (2001). Fluvial tufa formation in hard-water creek. Deinschwanger Bach, Franconian Al. *Germany. Facies, 44*, 1–22.

Auqué, L., Arenas, C., Osácar, C., Pardo, G., Sancho, C., & Vázquez-Urbez, M. (2014). Current tufa sedimentation in a changing-slope valley: The River Añamaza (Iberian Range, NE Spain). *Sedimentary Geology, 303*, 26–48.

Azennoud, K., Baali, A., Brahim, Y. A., & Ahouach, Y. (2021). Climate controls on tufa deposition over the last 5000 years: A case study from Northwest Africa. *Palaeogeography, Palaeoclimatology, Palaeoecology, 586*, 110767. https://doi.org/10.1016/j.palaeo.2021.110767

Bertini, A., Minissale, A., & Ricci, M. (2014). Palynological approach in upper Quaternary terrestrial carbonates of central Italy: Anything but a "mission impossible". *Sedimentology, 61*, 200–220. https://doi.org/10.1111/sed.12079

Buccino, G., D'Argenio, B., Ferreri, V., Brancaccio, L., Panichi, C. & Stanzione, D. (1978). Il travertini della bassa Valle del Tanagrio (Campania): Studio geomorphologico, sedimentologico e geochimico. *Bolletino della Societá Geologica Italiana*, *97*, 617–646.

Cacho, I., Grimalt, J. O., & Canals, M. (2002). Response of the Western Mediterranean Sea to rapid climatic variability during the last 50,000 years: A molecular biomarker approach. *Journal of Marine Systems, 33*(34), 253–272.

Capezzuoli, E., Gandin, A., & Pedley, H. M. (2009). *Travertines and calcareous tufa in Tuscany (Central Italy) Fieldtrip Guidebook* (pp. 129–158). 27th IAS Meeting of.

Capezzuoli, E., Gandin, A., & Pedley, M. (2014). Decoding tufa and travertine (fresh water carbonates) in the sedimentary record: The state of the art. *Sedimentology, 61*, 1–21.

Capezzuoli, E., Gandin, A., & Sandrelli, F. (2010). Calcareous tufa as indicators of climatic variability: A case study from southern Tuscany (Italy). In H. M. Pedley & M. Rogerson (Eds.), *Tufas and Speleothems: Unravelling the microbial and physical controls* (Vol. 336, pp. 263–281). Geological Society, Special Publications.

Carreira, P. M., Nunes, D., Valério, P., & Araújo, M. F. (2009). A 15-year record of seasonal variation in the isotopic composition of precipitation water over continental Portugal. *Journal of Radioanalytical and Nuclear Chemistry, 281*, 153–156. https://doi.org/10.1007/s10967-009-0064-0

Carthew, K. D., Taylor, M. P., & Drysdale, R. N. (2003). Are current models of tufa sedimentary environments applicable to tropical systems? A case study from the Gregory River. *Sedimentary Geolology, 162*, 199–218.

Chafetz, H. S., Utech, N. M., & Fitzmaurice, S. P. (1991). Differences in the $\delta^{18}O$ and $\delta^{13}C$ signatures of seasonal laminae comprising travertine stromatolites. *Journal of Sedimentary Petrology, 61*, 1015–1028.

Chen, J., Zhang, D. D., Shijie, W., Tangfu, X., & Ronggui, H. (2004). Factors controlling tufa deposition in natural waters at waterfall sites. *Sedimentary Geolology, 166*, 353–366.

Choffat, P. (1895). Notes sur les Tufs de Condeixa et la découverte de I'hippopotame en Portugal. *Com. Dir. Serv. Geol. Portugal*, *III*, 1–12 Lisboa.

Cremaschi, M., Zerboni, A., Spötl, Ch., & Felletti, F. (2010). The calcareous tufa in the Tadrart Acacus Mt. (SW Fezzan, Libya). An early Holocene palaeoclimate archive in the central Shahara. *Palaeogeography Palaeoclimatology Palaeoecology, 287*, 81–94.

Cunha, P. P., Martins, A. A., & Gouveia, M.P. (2016). As escadarias de terraços do Ródão à Chamusca (Baixo Tejo)—Caracterização e interpretação de dados sedimentares, tectónicos, climáticos e do Paleolítico. *Estudos do Quaternário*, *14*, APEQ, Braga, 1–24. http://www.apeq.pt/ojs/index.php/apeq.

Della Porta, G. (2015). Carbonate build-ups in lacustrine, hydrothermal and fluvial settings: Comparing depositional geometry, fabric types and geochemical signature. In D. W. J. Bosence, K. A. Gibbons, D. P. Le Heron, W. A. Morgan, T. Pritchard, & B. A. Vining (Eds.), *Microbial carbonates in space and time: Implications for global exploration and production* (Vol. 418, pp. 17–68). Geological SocietySpecial Publications.

Deocampo, D. M. (2010). The geochemistry of continental carbonates. In A. M. Alonso-Zarza & L. H. Tanner (Eds.), *Carbonates in continental settings, geochemistry, diagenesis, and applications. Developments in sedimentology* (Vol. 62, pp. 1–59). Elsevier.

Drysdale, R. N., Taylor, M. P., & Ihlenfeld, C. (2002). Factors controlling the chemical evolution of travertine-depositing rivers of the Barkly karst, Northern Australia. *Hydrological Processes, 16*, 2941–2962.

Duarte, M. L. & Bento dos Santos, T. M. (2010). *Carta Geológica de Portugal à escala 1:1,000,000*, edição 2010, Unidade de Geologia e Cartografia Geológica. LNEG-LGM, Lisbon, Portugal.

Durán, J. J. (1989). Geocronología de los depósitos asociados al karst en España. In J. J. Durán & J. López-Martínez (Eds.), *El karst en España* (Vol. 4, pp. 243–256). Sociedad Española de Geomorfología. Monograph.

Faure, G. (1998). *Principles and applications of geochemistry*. Prentice Hall, Inc.

Fernandes, J. P. (2018). *As Grutas de Lapas. Ensaio sobre lapas e abrigos escavados em tufos calcários dos terraços quaternários do rio Almonda*. Coleção Estudos e Documentos vol 11. Câmara Municipal de Torres Novas, Portugal. p. 116

Fino, A. R. F. (2018). Avaliação de Alguns Elementos Climáticos na Região do Ribatejo. Instituto Politécnico de Santarém (Portugal). Master Degree, ProQuest Dissertations Publishing, Samtarém, Portugal.

Flyche, M. (1907). Note sur les empreintes végétales de Pernes. In F. Roman & Torres, A., Le Néogéne continental dans la basse vallée du Tage (rive droite). Mem. Com. Serv. Geol. de Portugal.

Ford, T. D., & Pedley, H. M. (1996). A review of tufa and travertine deposits of the world. *Earth Science Reviews, 41*(3–4), 17–175.

Gibbard, P. L., Boreham, S., Cohen, K. M., & Moscariello, A. (2005). Global chronostratigraphical correlation table for the last 2.7 million years. *Boreas, 34*.

Gradziński, M. (2010). Factors controlling growth of modern tufa: Results of a field experiment. In H. M. Pedley & M. Rogerson (Eds.), *Tufas and Speleothems: Unravelling the microbial and physical controls* (Vol. 336, pp. 143–191). Geological Society, Special Publications.

Guerreiro, P., Cunha, L., Ribeiro, C., & Candeias, A. (2010). Os tufos calcários das áreas de Estoi, Loulé e ribeira das Mercês (Algarve, Portugal): caracterização e significado paleoambiental. *e-Terra*, *21* (7), 4. http://e-terra.geopor.pt

Guerreiro, P., Cunha, L., & Ribeiro, C. (2013). Caracterização geomorfológica e sedimentológica dos tufos calcários no flanco Sul da flexura de Algibre, Algarve Central (Portugal). Atas do VI Congresso Nacional de Geomorfologia. Coimbra, Portugal. pp. 4–7

Guerreiro, P. M. O. (2015). Tufos calcários no Algarve central: geomorfologia, sedimentologia e paleoambientes. Tese de doutoramento. Coimbra, Portugal. http://hdl.handle.net/10316/26296

Hearty, P. J., O'Leary, M. J., Kaufman, D. S., Page, M. C., & Bright, J. (2004). Amino acid geochronology of individual foraminifer (Pulleniatina obliquiloculata) tests, north Queenland margin, Australia: a new approach to correlating and dating Quaternary tropical marine sediment cores. *Paleoceanography, 19*, 4022. https://doi.org/10.1029/2004PA001059

Henchiri, M. (2014). Quaternary paludal tufas from the Ben Younes spring system, Gafsa, southwestern Tunisia: interactions between tectonics and climate. *Quaternary International, 338*, 71–87. https://doi.org/10.1016/j.quaint.2013.12.024

Henning, G. J., Grün, R., & Brunnacker, K. (1983). Speleothems, travertines and paleoclimates. *Quaternary Research, 20*, 1–29. https://doi.org/10.1016/0033-5894(83)90063-7

IAEA (2005). *Isotopic composition of precipitation in the Mediterranean Basin in relation to air circulation patterns and climate.* Final report of a coordinated research project 2000–2004. International Atomic Energy Agency, Austria. p. 223

Kano, A., Hagiwara, R., Kawai, T., Hori, M., & Matsuoka, J. (2007). Climatic conditions and hydrological change recorded in a high-resolution stable-isotope profile of a recent laminated tufa on a subtropical island, southern Japan. *Journal of Sedimentary Research, 77*, 59–67.

Kaufman, D. S. (2000). Amino acid racemization in ostracodes. In G. A. Goodfriend, M. J. Collins, M. L. Fogel, S. A. Macko, & J. F. Wehmiller (Eds.), *Perspectives in amino acids and protein geochemistry* (pp. 145–160). Oxford University Press.

Kaufman, D. S. (2003). Amino acid paleothermometry of Quaternary ostracodes from the Bonneville Basin, Utah. *Quaternary Science Reviews, 22*, 899–914.

Kaufman, D. S. (2006). Temperature sensitivity of aspartic and glutamic acid racemization in the foraminifera Pulleniatina. *Quaternary Geochronology, 1*, 188–207.

Kaufman, D. S., & Manley, W. F. (1998). A new procedure for determining DL amino acid ratios in fossils using reverse phase liquid chromatography. *Quaternary Geochronology, 17*, 987–1000.

Kawai, T., Kano, A., Matsuoka, J., & Ihara, T. (2006). Seasonal variation in water chemistry and depositional processes in a tufa-bearing stream in SW-Japan, based on 5 years of monthly observations. *Chemical Geology, 232*, 33–53.

Kele, A., Sallam, E. S., Capezzuoli, E., Rogerson, M., Wanas, H., Shen, C. C., Lone, M. A., Yu, T. L., Shauer, A., & Huntington, K. W. (2021). Were springline carbonates in the Kurkur-Dungul area (southern Egypt) deposited during glacial periods? *Journal of the Geological Society*. https://doi.org/10.1144/jgs2020-147

Kosnik, M. A., & Kaufman, D. S. (2008). Identifying outliers and assessing the accuracy of amino acid racemization measurements for geochronology: II. *Data Screening. Quaternary Geochronology, 3*, 328–341.

Leng, M. J., & Marshall, J. D. (2004). Palaeoclimate interpretation of stable isotope data from lake sediment archives. *Quaternary Science Reviews, 23*, 811–831.

Liu, Z., Svensson, U., Dreybrodt, W., Daoxian, Y., & Buhmann, D. (1995). Hydrodynamic control of inorganic calcite precipitation in Huanglong Ravine, China: Field measurement and theoretical prediction of deposition rates. *Geochimica Et Cosmoschimica Acta, 59*, 3087–3097.

Manuppella, G., Antunes, M. T., Almeida, C. A., Azerêdo, A. C., Barbosa, B., Cardoso, J. L., Crispim, J. A., Duarte, L. V., Henriques, M. H., Martins, L. T., Ramalho, M. M., Santos, V., & Terrinha, P. (2000). Carta Geológica de Portugal, 1:50.000, *Notícia Explicativa da Folha* n. 27–A (Vila Nova de Ourém). Departamento de Geologia, Instituto Geológico e Mineiro. Lisboa. p. 89

Manuppella, G., Barbosa, B., Azerêdo, A. C., Carvalho, J., Crispim, J., Machado, S., & Sampaio, J. (2006). Carta Geológica de Portugal, 1:50.000, *Notícia Explicativa da Folha* n. 27–C (Torres Novas), 66 p. Departamento de Geologia, Instituto Nacional de Engenharia, Tecnologia e Inovação. Lisboa.

Martín Algarra, A., Martín-Martín, M., Andreo, B., Julià, R., & González-Gómez, C. (2003). Sedimentary patterns in perched spring travertines near Granada (Spain) as indicators of the paleohydrological and paleoclimatological evolution of a karst massif. *Sedimentary Geology, 161*, 217–228. https://doi.org/10.1016/S0037-0738(03)00115-5

Martínez Tudela, A., Robles Cuenca, F., Santisteban Bové, C., Grün, R., & Hentzsch, B. (1986). Los travertinos del Río Matarraña, Beceite (Teruel), como indicadores paleoclimáticos del Cuaternario. In F. L. Vera (Ed.), *Quaternary climate in western mediterranean* (pp. 307–324). Universidad Autónoma de Madrid.

Martins, A. A., Cunha, P. P., Matos, J., & Guiomar, N. (2008). Correlação dos terraços do rio Tejo, no troço entre Gavião e Chamusca, por cartografia geomorfológica e datações por luminescência. IV Congresso Nacional de Geomorfologia. Braga, Portugal. p. 25

Martins, A. A. & Cunha, P. P. (2009). Terraços do rio Tejo em Portugal, sua importância na interpretação da evolução da paisagem e da ocupação humana. In *Arqueologia do Vale do Tejo*, Centro Português de Geo-História e Pré-História, Lisboa. pp. 163–176, http://hdl.handle.net/10316/15161

McCrea, J. M. (1950). On the isotope chemistry of carbonates and a paleotemperature scale. *Journal of Chemical Physics*, *18*, 849–857.

Mendes, A. G. (1974). Os tufos de Condeixa: estudo de Geomorfologia. *Cadernos de Geografia*. Instituto de Estudios Geográficos. Faculdade de Letras, Universidade de Coimbra, Coimbra. 4, 53–119

Miall, A. D. (1978). Lithofacies types and vertical profile models in Braided river deposits: A summary. In A. D. Miall (Ed.), *Fluvial sedimentology* (Vol. 5, pp. 597–604). Canadian Society of Petroleum Geologists. Memoir.

Moeyersons, J., Nyssen, J., Poesen, J., Deckers, J., & Haile, M. (2006). Age and backfill/overfill stratigraphy of two tufa dams, Tigray Highlands, Ethiopia: Evidence for Late Pleistocene and Holocene wet conditions. *Palaeogeography, Palaeoclimatology, Palaeoecology, 230*, 165–181. https://doi.org/10.1016/j.palaeo.2005.07.013

Ordóñez, S., Cuevas, J., Benavente, D., & García-del-Cura, M. A. (2016). Architecture of Pleistocene fluvial tufa systems associated with waterfalls: El Salt (Alcoy, Spain). *Geogaceta, 59*, 7–10.

Ordóñez, S., González Martín, J. A., García del Cura, M. A., & Pedley, H. M. (2005). Temperate and semi-arid tufas in Pleistocene to Recent fluvial barrage system in the Mediterranean area: The Ruidera Lakes Natural Park (Central Spain). *Geomorphology, 69*, 332–350.

Ortiz, J. E., Torres, T., Delgado, A., Reyes, E., & Díaz-Bautista, A. (2009). A review of the Tagus river tufa deposits (central Spain): Age and palaeoenvironmental record. *Quaternary Science Reviews, 28*, 947–963.

Ortiz, J. E., Torres, T., Delgado, A., Reyes, E., Llamas, J. F., Soler, V., & Raya, J. (2006). Pleistocene paleoenvironmental evolution at continental middle latitudes inferred from carbon and oxygen stable isotope analysis of ostracods from the Guadix-Baza Basin (Granada, SE Spain). *Palaeogeography, Palaeoclimatology, Palaeoecology, 240*, 535–561.

Ortiz, J. E., Torres, T., Julià, R., Delgado, A., Llamas, F. J., Soler, V., & Delgado, J. (2004). Numerical dating algorithms of amino acid racemization ratios from continental ostracodes. Application to Guadix-Baza basin (southern Spain). *Quaternary Science Reviews, 23*(5–6), 717–730.

Ortiz, J. E., Torres, T., & Pérez-González, A. (2013). Amino acid racemization in four species of ostracodes: Taxonomic, environmental, and microstructural controls. *Quaternary Geochronology, 16*, 129–143.

Ortiz, J. E., Torres, T., Ramallo, S. F., & Ros, M. (2015). Algoritmos de datación por racemización de aminoácidos de ostrácodos del Holoceno y Pleistoceno superior en la Península Ibérica. *Geogaceta, 58*, 59–62.

Osácar, M. C., Arenas, C., Vázquez-Urbez, M., Sancho, C., Auqué, L. F., & Pardo, G. (2013). Environmental Factors Controlling the $\delta^{13}C$ and $\delta^{18}O$ Variations of Recent Fluvial Tufas: A 12-Year Record from the Monasterio de Piedra Natural Park (Ne Iberian Peninsula). *Journal of Sedimentary Resesearch, 83*, 309–322.

Özkul, M., Gökgöz, A., & Horvatincic, N. (2010). Study from the Denizli Province, Western Turkey springline tufa deposits and associated spring waters: A case study from the Denizli Province, Western Turkey. In H. M. Pedley & M. Rogerson (Eds.), *Tufas and Speleothems: Unravelling the microbial and physical controls* (Vol. 336, pp. 245–262). Geological SocietySpecial Publications. https://doi.org/10.1144/SP336.13

Pedley, H. M. (1990). Classification and environmental models of cool freshwater tufas. *Sedimentary Geology, 68*, 143–154.

Pedley, H. M., González-Martín, J. A., Ordóñez, S., & García del Cura, M. A. (2003). Sedimentology of Quaternary perched springline and paludal tufas: Criteria for recognition, with examples from Guadalajara Province, Spain. *Sedimentology, 50*, 23–44.

Pedley, M. (2009). Tufas and travertines of the Mediterranean region: A testing ground for freshwater carbonate concepts and developments. *Sedimentology, 56*, 221–246.

Pedley, M., Andrews, J., Ordoñez, S., García del Cura, M. A., González Martín, J. A., & Taylor, D. (1996). Does climate control the morphological fabric of freshwater carbonates? A comparative study of Holocene barrage tufas from Spain and Britain. *Palaeogeography Palaeoclimatology Palaeoecology, 121*, 239–257.

Peña, J. L., Sancho, C., & Lozano, M. V. (2000). Climatic and tectonic significance of Late Pleistocene and Holocene tufa deposits in the Mijares River Canyon, eastern Iberian Range, northeast Spain. *Earth Surface Processes and Landforms, 25*, 1403–1417.

Pentecost, A. (2005). *Travertine*. Springer-Verlag.

Pentecost, A., & Spiro, B. (1990). Stable carbon and oxygen isotope composition of calcites associated with modern freshwater cyanobacteria and algae. *Geomicrobiology Journal, 8*, 17–26.

Queiroz, P.F., & Mateus, J. E. (2011). *Estudo polínico dos tufos calcários da ribeira da Asseca, Tavira—Relatório Final (Terras Scenica—Território Antigo, 24)*. Projeto HOLOCLIMA. 23 p. Lisboa.

Renaut, W. R., Owen, B., Jones, B., Tiercelen, J. J., Ego, J. K., & Konhauser, K. O. (2013). Impact of lake-level changes on the formation of thermogene travertine in continental rifts: Evidence from Lake Bogoria, Kenya Rift Valley. *Sedimentology, 60*, 428–468. https://doi.org/10.1111/j.1365-3091.2012.01347.x

Ribeiro, C., Terrinha, P., Voelker, A., Candeias, A., Rosado, L., & Guerreiro, P. (2013). The Holocene Climatic Recovery in SW Iberia Preserved in Limestone Tuff Deposits. Ciências da Terra (UNL), nº especial. 1st International Congress on Stratigraphy. Lisboa. 7, 1

Ribeiro, C., Terrinha, P., Voelker, A., Candeias, A., Rosado, L., & Guerreiro, P. (2014). The Holocene Climatic Recovery in South-Western Iberia as recorded in Limestone Tuff Deposits. In R. Rocha, J. Pais, J. C. Kullberg, & E. S. Finney (Eds.), *At the Cutting Edge of Stratigraphy* (pp. 869–872). Springer.

Ricci, M., Bertini, A., Capezzuoli, E., Horvatinčić, N., Andrews, J. E., Fauquette, S., & Fedi, M. (2015). Palynological investigation of a Late Quaternary calcareous tufa and travertine deposit: The case study of Bagnoli in the Valdelsa Basin (Tuscany, central Italy). *Review of Palaeobotany and Palynology, 218*, 184–197.

Rodríguez-Berriguete, A., Alonso-Zarza, A. M., Martín-García, R., & Cabrera, M. C. (2018). Sedimentology and geochemistry of a human-induced tufa deposit: Implications for palaeoclimatic research. *Sedimentology, 65*, 2253–2277.

Rodríguez-Berriguete, A., Camuera, J., & Alonso-Zarza, A. M. (2021). Carbonate tufas as archives of climate and sedimentary dynamic in volcanic settings, examples from Gran Canaria (Spain). *Sedimentology, 69*, 199–218.

Roiron, P. (1997). Apport des flores de travertins à la reconstitution des paléoenvironnements néogenes et quaternaires. *Études de Géographie Physique*, *Supl. au Nº XXVI*, 39–42.

Rubio-Millán, C. (2002). Estudio paleobotánico en tobas carbonatadas del Cuaternario de la localidad de Cañizar del Olivar (Teruel). *Teruel, 88–89*, 157–177.

Sallam, E. S. (2022). Facies and early diagenesis of rainwater-fed paleospring calcareous tufas in the Kurkur oasis area (southern Egypt). *Carbonates and Evaporites, 37*, 46. https://doi.org/10.1007/s13146-022-00792-3

Sancho, C., Arenas, C., Vázquez-Urbez, M., Pardo, G., Lozano, M. V., Peña-Monné, J. L., Hellstrom, J., Ortiz, J. E., Osácar, M. C., Auqué, L., & Torres, T. (2015). Climatic implications of the Quaternary fluvial tufa record in the NE Iberian Peninsula over the last 500 ka. *Quaternay Research, 84*(3), 398–414.

Santos, J. G. (1996). *A depressão marginal. Elementos para a caracterização geomorfológica do sector Coimbra-Penela e análise de riscos de movimentos de terreno*. Dissertação de Mestrado em Geografia Física. Faculdade de Letras da Universidade de Coimbra, Coimbra. p. 214

Santos, A., & Reis, M. (2021). *As manifestações parietais do complexo subterrâneo das Grutas de Lapas*. Análise preliminar. Fundação Côa Parque.

Soares, A. F., Cunha, L., & Marques, J. F. (1997). Les tufs calcaires dans la région du Baixo Mondego (portugal). *Études de Géographie Physique*, *suppl. nº XXVI*, 55–58.

Stone, A., Inglis, R., Barfod, D., Ickert, R., Hughes, L., Waters, J., Jourdan, A. L., & Alsharekh, A. M. (2022). Hydroclimatic and geochemical palaeoenvironmental records within tufa: A cool-water fluvio-lacustrine tufa system in the Wadi Dabsa volcanic setting, western Saudi Arabia. *Sedimentary Geology, 437*, 106181.

Thomas, C. (1985). Grottes et algares du Portugal. Lisboa Gráf. Eurograf, p. 227. http://purl.pt/14457.

Töker, E. (2017). Quaternary fluvial tufas of Sarıkavak area, southwestern Turkey: Facies and depositional systems. *Quaternary International, Non-Marine Carbonates, Special Issue, 437*, 37–50.

Torres, T., Llamas, J., Canoira, L., García-Alonso, P., García-Cortés, A., & Mansilla, H. (1997). Amino acid chronology of the Lower Pleistocene deposits of Venta Micena (Orce, Granada, Andalusia, Spain). *Organic Geochemistry, 26*, 85–97.

Torres, T., Ortiz, J. E., García de la Morena, M. A., Llamas, F. J., & Goodfriend, G. (2005). Aminostratigraphy and aminochronology of a tufa system in Central Spain. *Quaternary Internacional, 135*, 21–33.

Valero-Garcés, B. L., Moreno, A., Navas, A., Mata, P., Machín, J., Delgado Huertas, A., González Sampériz, P., Schwalb, A., Morellón, M., Cheng, H., & Edwards, R. L. (2008). The Taravilla lake and tufa deposits (Central Iberian Range, Spain) as palaeohydrological and palaeoclimatic indicators. *Palaeogeography, Palaeoclimatology, Palaeoecology, 259*, 136–156. https://doi.org/10.1016/j.palaeo.2007.10.004

Vázquez-Urbez, M., Arenas, C., & Pardo, G. (2012). A sedimentary facies model for stepped, fluvial tufa systems in the Iberian Range (Spain): The Quaternary Piedra and Mesa valleys. *Sedimentology, 59*, 502–526.

Vázquez-Urbez, M., Arenas, C., Sancho, C., Auqué, L. F., Osácar, C., & Pardo, G. (2011). Quaternary and present-day tufa systems of the Rivers Piedra and Añamaza (Iberian Range, Spain). In C. Arenas, L. Pomar, & F. Colombo (Eds.), *Post-meeting field trips guidebook, 28th IAS Meeting* (Vol. 8, pp. 241–274). Geo-Guías Sociedad Geológica de España.

Viles, H. A., & Pentecost, A. (2007). Tufa and travertine. In D. Nash & S. McLaren (Eds.), *Geochemical sediments and landscapes* (pp. 173–199). Blackwell Publishing. https://doi.org/10.1002/9780470712917

Viles, H. A., Taylor, M. P., Nicoll, K., & Neumann, S. (2007). Facies evidence of hydroclimatic regime shifts in tufa depositional sequences from the arid Naukluft Mountains, Namibia. *Sedimentary Geology, 195*, 39–53.

Violante, C., Ferreri, V., D'Argenio, B., & Golubic, S. (1994). Quaternary travertines at Rocchetta a Volturno (Isernia, central Italy). Facies analysis and sedimentary model of an organogenic carbonate system. Excursion A1, 21 pp. 15th IAS Regional Meeting, Ischia, Italy.

Zbyszewski, G., Manuppella, G., Da Veiga Ferreira, O., Mouterde, R., Ruget-Perrot, Ch., & Torre de Assunção, C. (1974) Notícia Explicativa da Carta Geológica de Portugal na escala de 1:50 000, Vila Nova de Ourém. Serviços Geológicos de Portugal.